Engineering NIR-Sighted Bacteria

Stefanie S. M. Meier[1,‡], Michael Hörzing[1,‡], Cornelia Böhm[2,3,‡], Emma L. R. Düthorn[1,‡], Heikki Takala[2,‡], René Uebe[4,5,‡], Andreas Möglich[1,5,6,*,‡]

[1] Department of Biochemistry, University of Bayreuth, 95447 Bayreuth, Germany.
[2] Department of Biological and Environmental Science, Nanoscience Center, University of Jyvaskyla, Jyvaskyla 40014, Finland.
[3] Institute of Biochemistry, Graz University of Technology, 8010 Graz, Austria
[4] Department of Microbiology, University of Bayreuth, 95447 Bayreuth, Germany.
[5] Bayreuth Center for Biochemistry & Molecular Biology, Universität Bayreuth, 95447 Bayreuth, Germany.
[6] North-Bavarian NMR Center, Universität Bayreuth, 95447 Bayreuth, Germany.

* for correspondence: andreas.moeglich@uni-bayreuth.de
‡ ORCID identifiers: S.S.M.M. 0009-0002-6028-5223; M.H. 0009-0008-2301-3783; C.B. 0000-0002-3552-2349; E.L.R.D. 0009-0000-4156-5428; H.T. 0000-0003-2518-8583; R.U. 0000-0003-2357-1589; A.M. 0000-0002-7382-2772

Abstract

Spatially and temporally orchestrated gene expression underpins organismal development, physiology, and adaptation. In bacteria, two-component systems (TCS) translate environmental cues into inducible expression outputs. Inducible expression also serves as a versatile implement in both basic and applied science. Here, we harness the photosensors of rhizobial bathy-phytochromes to construct synthetic TCSs for stringent activation of gene expression by near-infrared (NIR) light in laboratory and probiotic *Escherichia coli* strains, and in *Agrobacterium tumefaciens*. Orthogonal TCSs afford the multiplexed expression control of several genes by NIR and visible light. Notwithstanding substantial photochemical activation of bathy-phytochromes by visible radiation, the NIR-light-responsive systems hardly responded to red light. Evidently, light signals can be processed by TCSs into highly nonlinear responses at the physiological relevant level of gene expression. These fundamental aspects likely extend to naturally occurring TCSs. Depending on their photosensor traits

28 and environmental conditions, bathy-phytochromes may thus either be NIR-specific or function as
29 colorblind receptors of light vs. darkness.

30 **Keywords**

31 bacterial phytochrome; gene expression; near-infrared light; optogenetics; sensor histidine kinase;
32 sensory photoreceptor; two-component system

33 **Introduction**

34 Proportionate to its essential roles in organismal physiology, development, replication, and
35 adaptation, gene expression is stringently and precisely regulated. Various cellular circuits integrate
36 cognate input signals and, in turn, ramp up or down the expression of target genes. Molecular
37 analyses of these circuits not only benefit fundamental research, but also, they underlie applications
38 in biotechnology and synthetic biology for the precise control of gene expression. Two-component
39 systems (TCS) are the predominant signal-transduction pathways by which bacteria and several
40 other organisms process environmental stimuli and convert them into intracellular gene-expression
41 responses (Buschiazzo and Trajtenberg, 2019; Parkinson and Kofoid, 1992). In their canonical form,
42 TCSs comprise as one component a membrane-spanning, homodimeric sensor histidine kinase (SHK)
43 that relays signals to the cell interior. SHKs generally consist of N-terminal extracellular/periplasmic
44 sensor and C-terminal cytosolic effector modules, the latter of which subdivide into the DHp
45 (dimerization and phospho-accepting histidine) and CA (catalytic) domains. In signal-dependent
46 manner, SHKs undergo autophosphorylation at a conserved, eponymous histidine residue to enable
47 subsequent phosphoryl-group transfer to an aspartic acid residue within the response regulator
48 (RR), i.e., the second TCS component. Once phosphorylated, the RR commonly dimerizes and is
49 thereby rendered capable of sequence-specific DNA binding and transcription initiation at target
50 promoters (Gao et al., 2019). As it is the overall levels of phosphorylated RR that govern the

51 physiological output of the TCS, many SHKs are bifunctional and also exert phosphatase in addition
52 to their kinase activities (Möglich et al., 2009; Russo and Silhavy, 1993). Exceedingly stringent and
53 steep regulatory responses can be achieved by finely balancing the opposing RR phosphorylation
54 and dephosphorylation reactions. Depending on the signal, one or the other of the two elementary
55 activities prevails, and the SHK consequently acts as either net kinase or net phosphatase. SHKs are
56 specific for their respective RRs, thus allowing the coexistence in a single cell of multiple TCSs with
57 minimal crosstalk (Laub and Goulian, 2007).

58 Among the plethora of known TCSs, certain representatives respond to light as their cognate
59 stimulus (Möglich, 2019; Ohlendorf and Möglich, 2022). Pertinent TCSs comprise soluble
60 photoreceptor SHKs that reside in the cytosol and absorb light at specific wavelengths within the
61 near-ultraviolet (UV) to near-infrared (NIR) range of the electromagnetic spectrum (Krell et al., 2010;
62 Möglich, 2019). Beyond their pivotal physiological role, these TCSs are of prime interest in
63 biotechnology as they unlock the control of gene expression by light, an approach belonging to
64 optogenetics (Deisseroth et al., 2006). As an inducer of gene expression, light brings several benefits
65 in that it affords superior spatial and temporal precision; can be applied, dosed, and withdrawn with
66 ease and in automatable fashion; and penetrates living tissue to a wavelength-dependent extent
67 (Weissleder, 2001). Several light-responsive TCSs have become available and support strong
68 regulatory responses covering the electromagnetic spectrum from the near-UV to the NIR (Lazar and
69 Tabor, 2021; Ohlendorf and Möglich, 2022). Apart from little-modified naturally occurring setups
70 (Tabor et al., 2011), additional photoreceptor SHKs have been engineered by modular recombination
71 of sensor and effector entities (Levskaya et al., 2005; Möglich et al., 2010, 2009). As a case in point,
72 the widely deployed pDusk and pDawn plasmids resort to the blue-light-inhibited SHK YF1
73 originating from the fusion of a light-oxygen-voltage (LOV) photosensor to the DHp/CA effector of
74 the *Bradyrhizobium japonicum* FixL SHK (Möglich et al., 2009; Ohlendorf et al., 2012). Irrespective

75 of the wealth of setups for the optical control of bacterial gene expression, there is a dearth of
76 circuits affording stringent responses to NIR light (Ong et al., 2018).

77 We previously expanded the pDusk plasmid family by exchanging said LOV photosensor for
78 photosensory core modules (PCM) of bacterial phytochromes (BphP) (Meier et al., 2024a;
79 Multamäki et al., 2022). The resultant pREDusk systems respond to red rather than blue light which
80 facilitates multiplexing (Meier et al., 2024b; Multamäki et al., 2022) with scores of bacterial
81 optogenetic circuits that mostly sense blue light (Ohlendorf and Möglich, 2022). As an added benefit,
82 red light penetrates mammalian tissue to a higher extent than blue light owing to reduced scattering
83 and absorption by cellular constituents, hemoglobin, and other pigments (Ash et al., 2017;
84 Weissleder, 2001). BphPs react to red and NIR light via biliverdin (BV) chromophores covalently
85 attached within their PCMs (Davis et al., 1999; Hughes et al., 1997; Takala et al., 2020). The linear
86 tetrapyrrole BV traverses between the *Z* and *E* isomers of its C15=C16 double bond which underpin
87 the red-absorbing Pr and the far-red-absorbing Pfr states of BphPs, respectively. Red and NIR light
88 triggers the photochromic *Z*/*E* isomerization of BV and thereby drives the photoconversion in the
89 Pr→Pfr and Pfr→Pr directions, respectively. In conventional BphPs, as in those underpinning the
90 pREDusk systems, the Pr state is the thermodynamically more stable form prevailing in darkness.
91 After red-light exposure, these BphPs revert to their Pr resting state thermally within the dark-
92 recovery reaction which is generally protracted and plays out over many hours to days. Conventional
93 BphPs therefore effectively act as ratiometric red/NIR-light sensors. In common with many natural
94 BphP-SHKs (Huber et al., 2024; Karniol and Vierstra, 2003; Lamparter et al., 2002; Multamäki et al.,
95 2021), the engineered ones in the pREDusk circuits exhibit net kinase activity towards their RR within
96 their Pr states and net phosphatase activity within their Pfr states. In pREDusk, red light therefore
97 downregulates target gene expression by several hundred-fold (Meier et al., 2024a; Multamäki et
98 al., 2022). More recently, we inverted the light response of the underlying BphP-SHKs by changing
99 the composition of the linkers through which their sensor and catalytic modules transduce signals

100 (Meier et al., 2024a). Doing so yielded BphP-SHKs with net kinase activity in their Pfr states and net
101 phosphatase activity in their Pr states, thus supporting pronounced increases of gene expression
102 under red light in the resultant pDERusk systems.

103 A second group of bacterial phytochromes, denoted bathy-BphPs, adopt the Pfr rather than
104 the Pr state in darkness (Karniol and Vierstra, 2003). Consequently, NIR light promotes the Pfr→Pr
105 conversion, as does visible light, if to a lesser degree. To the extent it has been studied, the thermal
106 dark recovery in bathy-BphPs is generally fast and complete within seconds to minutes. Due to these
107 aspects, bathy-BphPs are considered to primarily serve as sensors of light vs. darkness rather than
108 of a specific light color (Huber et al., 2024).

109 Informed by spectroscopic analyses, we here harness the PCMs of select bathy-BphPs for
110 stringently controlling TCS output and bacterial gene expression by NIR light. The resultant plasmid
111 systems, dubbed pNIRusk, prompt stringent upregulation of gene expression under NIR light. Equally
112 advantageously and unexpectedly, the engineered pNIRusk circuits show only minimal activation by
113 red light. To enable multiplexed applications, we also advance light-regulated setups based on
114 orthogonal TCSs. The pNIRusk plasmids not only afford pronounced NIR-light responses in
115 *Escherichia coli* laboratory strains but also in the probiotic Nissle bacteria and in *Agrobacterium*
116 *tumefaciens*. Taken together, we deliver versatile implements for the precision control of gene
117 expression by NIR light in both fundamental and applied research.

118 Results

119 Bathy-Bacteriophytochromes as Sensors of Light and pH

120 To subject bacterial gene expression to NIR light, we considered the PCMs of previously reported
121 bathy-BphPs as input modules (Rottwinkel et al., 2010; Tasler et al., 2005). To better inform our
122 choice, we expressed, purified, and spectroscopically characterized BphP PCMs from *Azorhizobium*

123 *caulinodans* (*Ac*PCM), *Agrobacterium vitis* (*Av*PCM), and *Pseudomonas aeruginosa* (*Pa*PCM).
124 Consistent with earlier reports, all three PCMs fully populated the Pfr state in darkness with distinct
125 Soret- and Q-band absorbance peaks at 415 nm and (755 ± 3) nm, respectively (Fig. 1a-c). Exposure
126 to NIR light drove the complete conversion to the Pr state characterized by maxima of the Soret band
127 at (393 ± 2) nm and of the Q band at around (698 ± 3) nm. Illumination with blue and red light
128 prompted partial population of the Pr state to around 65-80% and 40-70%, respectively. Strikingly,
129 at pH 8.0, the Q-band intensity of the pure Pr state differed markedly across the PCMs, with *Pa*PCM
130 showing the strongest signal, and *Ac*PCM the weakest. Based on earlier reports, these data may
131 principally reflect differences in BV protonation at the pyrrole C ring (Borucki et al., 2005; Zienicke
132 et al., 2013). To put this notion to the test, we recorded absorbance spectra for the three PCMs at
133 pH values between 6 and 11 (Fig. 1d-f). While the Q-band intensity remained invariant within the
134 Pfr state, in the Pr state it increased with decreasing pH. By evaluating the corresponding absorbance
135 peak heights as a function of pH, we determined apparent pK_a values of 7.2 ± 0.1, 8.0 ± 0.1, and 9.9
136 ± 0.2 for *Ac*PCM, *Av*PCM, and *Pa*PCM, respectively (Fig. 1g). Following previous studies (Zienicke et
137 al., 2013), we tentatively ascribe these pK_a values to (de-)protonation of the nitrogen atom within
138 the pyrrole C ring in BV. In addition, pH also affects the photostationary Pr:Pfr ratio under red light
139 which increases with rising alkalinity (Fig. 1h, Suppl. Fig. 1a-c).

140 Having ascertained the bathy-character of the candidate PCMs and their Pr⇄Pfr
141 interconversion, we next assessed the kinetics of reversion to their dark-adapted Pfr state at pH 8.0
142 following NIR illumination (Fig. 1i). All three PCMs fully recovered to the Pfr state in single-
143 exponential fashion, but the time constants τ for *Ac*PCM and *Av*PCM of (140 ± 1) s and (80 ± 1) s
144 were markedly lower than the value of (610 ± 1) s for *Pa*PCM. Closely similar recovery time constants
145 resulted after exposing the samples to red instead of NIR light (Suppl. Fig. 1d-e). With rising alkalinity,
146 we observed slower and less complete recovery after NIR-light exposure (Suppl. Fig. 1g-l).

147 Potentially, this deceleration directly owes to BV deprotonation evidenced in the absorbance
148 spectra. That is because BV remains protonated in the Pfr state across all investigated pH values, but
149 within the Pr state it is progressively deprotonated at higher pH values. The return to the Pfr state
150 hence requires re-protonation at elevated pH values which may slow down the dark recovery.

151 **Subjecting Bacterial Gene Expression to NIR-Light Control**

152 To achieve control of bacterial expression by NIR light, we adapted the previous *Dm*REDusk plasmid
153 which encodes a red-light-responsive chimeric SHK originating from the fusion of the PCM of
154 *Deinococcus maricopensis* BphP (*Dm*BphP) to the DHp/CA fragment of *B. japonicum* FixL (Meier et
155 al., 2024a). As not least seen in the above spectroscopic experiments, bathy-BphPs also respond to
156 visible besides NIR light, which stands to cause undesired crosstalk with genetic circuits that react
157 to, e.g., blue or red light. We reasoned that this adverse effect may be ameliorated by deliberately
158 rendering the NIR-responsive systems comparatively insensitive to light. Guided by the above
159 spectroscopic analyses, we selected *Ac*PCM and *Av*PCM as they exhibit a faster Pr→Pfr dark recovery
160 than *Pa*PCM, which translates into a lower effective light sensitivity at photostationary state
161 (Ohlendorf and Möglich, 2022; Ziegler and Möglich, 2015).

162 With *Ds*Red as a fluorescence reporter gene, we replaced *Dm*PCM within *Dm*REDusk by
163 either *Ac*PCM or *Av*PCM, while maintaining the same register for the linker between the PCM and
164 DHp/CA moieties (Suppl. Fig. 2). In the resultant plasmids, referred to as pNIRusk, the heme
165 oxygenase enzyme for intracellular BV provision, the BphP-SHK, and the matching RR FixJ thus form
166 a constitutively expressed tricistronic operon (Fig. 2a). The initial pNIRusk designs, denoted '0',
167 showed constant reporter fluorescence, largely independent of illumination, despite their BphP-
168 SHKs adhering to the same design as in *Dm*REDusk (Fig. 2b).

169 Spurred by our recent construction of the pDERusk setups (Meier et al., 2024a), we
170 hypothesized that light responsiveness may be installed by varying the composition of the linker
171 between the PCM and DHp/CA moieties. Using the PATCHY approach (Ohlendorf et al., 2016), we
172 generated libraries of the *Ac*NIRusk and *Av*NIRusk setups that differ in the length and sequence of
173 said linker. By assessing the reporter fluorescence in darkness and under NIR and red light, we
174 identified five light-switchable variants for *Ac*NIRusk and six for *Av*NIRusk (Fig. 2b, Suppl. Fig. 3). We
175 refer to individual variants by their linker lengths relative to the initial constructs. Although the light-
176 responsive variants all rely on the same PCMs and DHp/CA modules, they drastically differed in their
177 response to NIR light, with some elevating and others lowering reporter-gene expression compared
178 to darkness. We subsequently focused on variants inducing gene expression under NIR light, albeit
179 with intriguing variation in their response to red light. For instance, *Ac*NIRusk-1b with a linker one
180 residue shorter than in *Dm*REDusk showed sizeable induction under red light. By contrast, the
181 variant *Ac*NIRusk-1a with the same linker length but different sequence did much less so. For an
182 eventual application, we deem a reduction of red-light-induced activation advantageous. We thus
183 continued with *Ac*NIRusk-1a and *Av*NIRusk+17a, both of which strongly induce expression under NIR
184 light compared to darkness but only show small responses to red light. For simplicity, we refer to
185 these setups as *Ac*NIRusk and *Av*NIRusk in the following.

186 Flow cytometry revealed homogeneous single-cell fluorescence distributions for *E. coli*
187 bacteria harboring *Ac*NIRusk or *Av*NIRusk (Fig. 2c). When incubated in darkness, the median
188 fluorescence was only 1.2-fold above the background fluorescence. Saturating NIR light (800 nm,
189 250 µW cm^{-2}) induced largely uniform shifts of the entire cell population to several 10-fold higher
190 median fluorescence for *Ac*NIRusk and *Av*NIRusk, respectively, an effect similar in magnitude to the
191 red-light response observed previously for the pDERusk systems (Meier et al., 2024a). At sub-

192 saturating light doses, the single-cell fluorescence of bacteria containing *Ac*NIRusk and *Av*NIRusk
193 uniformly rose to intermediate levels with increasing NIR-light intensity (Suppl. Fig. 4-5).

194 At the ensemble level, the average fluorescence per cell density ramped up sigmoidally with
195 NIR light by up to around 70- and 150-fold for *Ac*NIRusk and *Av*NIRusk, respectively (Fig. 2d-e). The
196 two systems exhibited half-maximal activation at relatively high NIR-light intensities of (29 ± 1) µW
197 cm^{-2} and (43 ± 1) µW cm^{-2}, i.e., about an order of magnitude above the half-maximal red-light doses
198 previously determined for induction of the pREDusk and pDERusk systems (Meier et al., 2024a;
199 Multamäki et al., 2022). Arguably, these differences reflect at least in part the respective dark-
200 recovery times of the underlying bathy-BphPs which are in the seconds to minutes range rather than
201 in the hours range for conventional BphPs.

202 Red light also induced *Ac*NIRusk and *Av*NIRusk but only around 2- and 6-fold relative to
203 darkness (Fig. 2d-e). Blue light elicited a stronger 16- and 25-fold induction, respectively, at the
204 highest probed light intensity of around 120 µW cm^{-2}. Higher blue-light intensities were not accessed
205 owing to instrumental limitations and onsetting phototoxicity. From the data, we determined half-
206 maximal blue-light doses of (46 ± 3) µW cm^{-2} and (100 ± 20) µW cm^{-2} for *Ac*NIRusk and *Av*NIRusk,
207 respectively. Given the around 1.7-fold higher energy of blue compared to NIR light, the circuits
208 therefore trigger at similar half-maximal photon fluencies for either light color. At least qualitatively,
209 the degree of induction by the individual light colors (red, blue, NIR) follows the same trend as the
210 photochemical responses evidenced in the underlying *Ac*PCM and *Av*PCM (see Fig. 1a-c) where NIR
211 light elicited the most pronounced Pr formation, followed by blue and red light.

212 **Engineering Orthogonal Light-responsive Two-Component Systems**

213 In common with earlier members of the pDusk pedigree, the pNIRusk systems are based on the FixLJ
214 TCS from *B. japonicum* (Anthamatten and Hennecke, 1991). Combinations of several of these setups

215 would hence experience crosstalk at the level of RR phosphorylation which, in all but a few cases, is
216 undesired. To overcome this limitation, we set out to engineer light-responsive TCSs orthogonal to
217 those used in pDusk, pNIRusk, and related setups. As recently surveyed, several TCSs have been
218 characterized to the point that they have found application in synthetic biology (Lazar and Tabor,
219 2021). Based on their reported stringency of regulation, we selected as candidate TCSs TtrSR from
220 *Shewanella baltica* that responds to tetrathionate and TodST from *Pseudomonas putida* that can
221 detect toluene compounds (Daeffler et al., 2017; Lau et al., 1997).

222 Starting from *Dm*REDusk, we substituted the original FixL DHp/CA domains for those from
223 TtrS, while also exchanging FixJ for the TtrR RR and putting the expression of a *Ds*Red reporter under
224 control of the Pttr promoter that is subject to regulation by TtrSR (Fig. 3a). Within this framework,
225 we then varied the linker interconnecting the *Dm*PCM and the TtrS DHp/CA module via PATCHY
226 (Ohlendorf et al., 2016). Screening of the resultant linker library for differential *Ds*Red expression
227 under darkness, and NIR and red light identified several variants, termed *Dm*Ttr, with substantial
228 light responses (Fig. 3a, Suppl. Fig. 6a). Notably, the overall expression levels within the identified
229 *Dm*Ttr systems were markedly higher than those in the pREDusk and pNIRusk setups.

230 Next, we extended the strategy to *Av*NIRusk by introducing TodST. Of note, TodS is a complex
231 SHK with integrated phosphorelay that comprises in sequential order PAS-1, DHp-1, CA-1, REC, PAS-
232 2, DHp-2, and CA-2 domains (Busch et al., 2009). Toluene signals, detected by PAS-1, modulate the
233 activity of the DHp-1/CA-1 unit which phosphorylates the REC domain that in turn governs the
234 activity of the DHp-2/CA-2 module and eventual phosphorylation of the TodT RR. Earlier reports
235 showed that a miniaturized TodS variant only comprising the PAS-1, DHp-2, and CA-2 domains,
236 dubbed mini-TodS, retains toluene sensitivity and stringent regulation of TodT (Silva-Jiménez et al.,
237 2012). Consequently, we replaced the FixLJ TCS in *Av*NIRusk by the TodS DHp-2/CA-2 fragment, while
238 also introducing the TodT RR and its cognate PtodX promoter (Fig. 3b). Linker variation by PATCHY

239 and screening for *Ds*Red reporter fluorescence pinpointed several variants, termed *Av*Tod, which
240 either elevated or lowered gene expression in response to NIR light (Fig. 3b, Suppl. Fig. 6b).

241 For further analyses, we selected the variants *Dm*Ttr+7b, *Av*Tod+16, and *Av*Tod+21 with PCM-
242 DHp/CA linkers 7, 16, and 21 residues, respectively, longer than that in the parental *Dm*REDusk
243 circuit. Exposed to red light, *Dm*Ttr+7b elicited an about 15-fold decrease of gene expression
244 compared to darkness (Suppl. Fig. 7a). Whereas *Av*Tod+16 supported a 20-fold reporter-
245 fluorescence decrease under NIR light, *Av*Tod+21 promoted an 8-fold increase of gene expression
246 (Suppl. Fig. 7b-c). Although the attained regulatory efficiencies pale in comparison to those of
247 *Dm*REDusk (Meier et al., 2024a) and *Av*NIRusk, the data show that the principal design and screening
248 strategies readily translate to other TCSs.

249 To allow multiplexing of several light-responsive circuits in a single bacterial cell, we modified
250 the *Dm*DERusk and *Av*NIRusk plasmids by replacing their kanamycin resistance marker, their ColE1
251 origin of replication (ori), and their *Ds*Red reporter gene by a streptomycin marker, the CloDF13 ori,
252 and the yellow-fluorescent YPet reporter, respectively. The resultant *Dm*DERusk-Str-YPet and
253 *Av*NIRusk-Str-YPet circuits showed similar responses to red and NIR light as the parental plasmids
254 they derive from (Suppl. Fig. 7d-e). Pairs of compatible plasmids with different TCSs, oris, resistance
255 markers, and fluorescent reporters were transformed into bacteria, followed by cultivation in
256 darkness, under red (100 µW cm^{-2}) or NIR light (200 µW cm^{-2}), or under both light colors. By
257 employing individual plasmid combinations, the expression of the *Ds*Red and YPet reporters could
258 be individually controlled by the two light colors (Fig. 3c, Suppl. Fig. 7f). For instance, when
259 combining *Dm*DERusk-Str-YPet with *Av*Tod+21-*Ds*Red, YPet and *Ds*Red expression rose under red and
260 NIR light, respectively, whereas the joint application of both light colors induced both reporter
261 genes. Taken together, well-chosen plasmid sets enable the orthogonal expression control of two
262 target genes by red and NIR light. Notably, the plasmids can be deployed as is with no further

263 modifications required. Rather than using saturating light intensities as in the above experiments,
264 yet finer-grained expression control can be exerted by adjusting the red- and NIR-light intensities.

265 **Applications in the Laboratory and Beyond**

266 As TCSs widely recur across bacterial phyla, they often retain functionality upon transfer between
267 different bacterial strains. Earlier reports not least demonstrated that representatives of the pDusk
268 family support light-regulated gene expression across several prokaryotes (Ohlendorf and Möglich,
269 2022). For instance, pDusk and its derivative pDawn (Ohlendorf et al., 2012) have been successfully
270 deployed in *E. coli* Nissle 1917 (*Ec*N) and other probiotic bacteria (Cui et al., 2021; Magaraci et al.,
271 2016; Pan et al., 2021; Sankaran and del Campo, 2019; Yang et al., 2020). These experiments augur
272 the application of light-responsive bacteria in the gut of mammals as programmable, living
273 therapeutics (Ohlendorf and Möglich, 2022). To date, however, pertinent applications are limited by
274 the shallow tissue penetration of blue light required for triggering pDusk and pDawn. Although
275 upconverting nanoparticles can be administered jointly with the light-responsive bacteria to allow
276 actuation by NIR light, this approach introduces complexity and departs from a fully self-contained,
277 optogenetic strategy (Yang et al., 2020). To assess whether the presently generated light-responsive
278 gene-expression systems may overcome this grave limitation, we introduced *Ac*NIRusk and *Av*NIRusk
279 into *Ec*N. Both setups mediated a more than 100-fold upregulation of reporter-gene expression
280 under NIR light with half-maximal doses of (27 ± 1) and (28 ± 2) µW cm^{-2}, respectively (Fig. 4a).

281 We next probed the performance of *Av*NIRusk and *Dm*REDusk in the biotechnologically
282 relevant *Agrobacterium tumefaciens*. To this end, we constructed derivative plasmids, denoted
283 *Av*NIRlux and *Dm*REDlux, that subject the expression of a luciferase operon under the control of the
284 light-responsive TCSs (Fig. 4b). After conjugational transfection into *A. tumefaciens*, the light
285 response was assessed by spotting the bacteria on agar plates (Fig. 4c). As visualized by
286 luminescence, the *Av*NIRlux system strongly induced expression upon incubation under NIR light

287 compared to darkness. Different from *E. coli* (see Fig. 2e, Suppl. Fig. 8a), red light activated to similar
288 extents as NIR light, whereas blue light induced expression only weakly. In the case of *Dm*REDlux,
289 the expression of the *lux* reporter was strongly reduced under both blue and red light, but not under
290 NIR light or in darkness. Although *A. tumefaciens* harbors two endogenous BphPs (Karniol and
291 Vierstra, 2003), our experiments did not detect any differences in growth or phenotype between
292 cultivation under NIR and red light. We next characterized the response of *A. tumefaciens* cultured
293 in liquid medium. Once reaching the stationary phase after around 20 h (Suppl. Fig. 8b), the cultures
294 bearing *Av*NIRlux exhibited a 7-fold activation of *lux* expression by NIR light compared to darkness.
295 For *Dm*REDlux, the *lux* expression was around 300-fold higher in darkness than under red light (Fig.
296 4d, Suppl. Fig. 8c-d).

297 **Discussion**

298 **Bathy-Bacteriophytochromes as Tunable Sensors of Light Intensity and Quality**

299 As conventional bacteriophytochromes do, bathy-BphPs transition between their Pr and Pfr states
300 with 15*Z*- and 15*E*-configured biliverdin, respectively. In marked contrast to the conventional
301 representatives, bathy-BphPs assume their 15*E*-configured Pfr state as the thermodynamically most
302 stable form in darkness, rather than their Pr state. Despite this principal difference, the overall PCM
303 architecture and the residues lining the bilin binding pocket are remarkably conserved across known
304 BphPs. Notwithstanding limited successes in reprogramming certain BphPs (Böhm et al., 2025; Xu et
305 al., 2024), the molecular determinants underlying bathy-character remain elusive and their design
306 demanding.

307 Owing to their Pfr dark-adapted state, bathy-BphPs undergo net Pfr→Pr conversion when
308 irradiated with light within the near-UV to NIR region of the electromagnetic spectrum. Put another
309 way, there is no light quality that would fully populate the dark-adapted Pfr state. Bathy-BphPs

310 surmount this challenge by a fast thermal Pr→Pfr recovery that restores the Pfr state within seconds
311 to minutes. The primary physiological role of bathy-BphPs may hence be that of sensors of light
312 quantity rather than quality (i.e., color) (Huber et al., 2024).

313 Intriguingly, we uncovered a profound pH influence on photoreception in bathy-BphPs. With
314 rising alkalinity, the absorption cross-section of the Q band strongly decreases within the Pr state
315 but remains unchanged for Pfr. Based on earlier studies (Borucki et al., 2005; Velazquez Escobar et
316 al., 2015; Zienicke et al., 2013), we attribute these spectral changes to (de-)protonation of the
317 nitrogen atom of the BV pyrrole C within the Pr state. The pertinent pK_a values range between 7-8
318 for *Ac*PCM and *Av*PCM, similar to the value of 7.6 for the bathy-BphP Agp2 from *A. tumefaciens*
319 (Zienicke et al., 2013), but substantially lower than the value of about 10 for *Pa*PCM. Inspection of
320 the experimentally determined *Pa*PCM and Agp2PCM structures in their Pfr states (Schmidt et al.,
321 2018; Yang et al., 2008) and the corresponding Pfr models for *Ac*PCM and *Av*PCM (Abramson et al.,
322 2024) reveals highly conserved chromophore-binding pockets with most residues adjacent to BV
323 identical in all four proteins (Suppl. Fig. 9). However, *Pa*PCM features tyrosine and serine residues at
324 positions 190 and 275 rather than phenylalanine and alanine, respectively, in the equivalent places
325 of the other three PCMs. Although speculative at present, these systematic differences may render
326 the *Pa*PCM binding pocket comparatively hydrophilic and thereby account for the divergent
327 protonation equilibrium of the pyrrole C ring.

328 BV deprotonation within the Pr state at elevated pH incurs at least three principal effects that
329 under constant light all promote population of the Pr state at the cost of the Pfr state. First, the
330 Pr→Pfr dark recovery slows down between pH 7 and 10 for all three investigated PCMs. At least in
331 part, this may reflect the need for BV re-protonation upon return from the Pr to the Pfr state which
332 remains fully protonated at all investigated pH values. Second, as noted above, BV deprotonation
333 leads to a drastic reduction of the Q-band absorbance within the Pr state (see Fig. 1). For a given
334 intensity of visible light, photoconversion to the Pfr state thus becomes less effective, thereby again

335 favoring the Pr state at photostationary state. Third, BV deprotonation also goes along with a
336 dramatic decrease in the apparent photoconversion quantum yields in the Pr→Pfr vs. the Pfr→Pr
337 directions (Suppl. Fig. 1f). As best exemplified for *Ac*PCM, at pH 6.5, the respective quantum yields
338 for the photoreversible Pr⇄Pfr interconversion are about equal, but at pH 10.5, the quantum yield
339 in the Pr→Pfr direction is less than 1% that in the Pfr→Pr direction. Together with the pH-dependent
340 reduction in the Pr-state Q-band absorbance, this mechanism leads to vastly different red-light-
341 induced photostationary states as a function of pH (see Fig. 1h). Whereas at low pH, saturating red
342 light results in about 60-70% Pfr population, at high pH values almost no Pfr state remains (Fig. 5).
343 As a direct consequence, at pH 10.5, red light counter-intuitively drives the complete conversion to
344 the Pr state of *Ac*PCM. Put another way, in its deprotonated form this bathy-BphP becomes
345 essentially colorblind and acts as a pure light-intensity sensor. Although less pronounced, *Av*PCM
346 and *Pa*PCM follow the same trend with pH.

347 While it is debatable whether the rhizobia *Ac*PCM and *Av*PCM derive from ever encounter
348 such extreme pH swings, it has been proposed that the resultant changes in photochemical
349 properties could serve a sensing function (Zienicke et al., 2013). Even independent of this aspect,
350 our present analyses show how pH impacts bathy-BphP photoreception at multiple levels. While it
351 remains true that all light colors net promote the Pfr→Pr transition, they do so to different extents
352 which can have a profound impact on downstream signal transduction as discussed below. We
353 propose that modulation of the BV protonation midpoint has been harnessed during evolution to
354 sculpt the light response of extant bathy-BphPs according to the individual needs of the respective
355 organism of origin. In line with this hypothesis, we presently evidence a considerable span of pK_a
356 values for BV protonation across several bathy-BphP PCMs.

357 **Engineering of NIR-Light-Responsive Proteins**

358 As best exemplified by sensor histidine kinases, PCMs of bathy-BphPs can occur in conjunction with
359 the same type of effector as those of conventional BphPs (Blum et al., 2025). However, it has been
360 unclear whether a single, specific output protein can be regulated in its activity by both PCM types.
361 The successful recombination of bathy-BphP PCMs with the same DHp/CA module earlier controlled
362 by conventional BphP PCMs (Meier et al., 2024a; Multamäki et al., 2022) now demonstrates the
363 principal validity of this idea. At least to some extent, the PCMs of conventional and bathy-BphPs are
364 hence interchangeable, a finding that indicates shared or compatible signal-transduction
365 mechanisms, as also suggested by the conserved structure and photochemistry across the BphP
366 class (Möglich, 2019; Takala et al., 2020). As one important ramification, numerous previously
367 engineered red-light-responsive receptors may thus be subjugated to NIR-light control by swapping
368 out their underlying PCMs from conventional BphPs for ones from bathy-BphPs (Chernov et al.,
369 2017; Etzl et al., 2018; Leopold et al., 2022, 2019; Levskaya et al., 2005; Schmidl et al., 2014; Stabel
370 et al., 2019; Stüven et al., 2019; Tang et al., 2021). Compared to the challenging approach of
371 imparting bathy-character via limited PCM modifications (Böhm et al., 2025; Xu et al., 2024), the
372 design task thus considerably simplifies.

373 We identify several caveats that likely hold for future design endeavors, too. Notably, the
374 connection between PCM and effector of choice needs to be conducive to transmitting light signals.
375 When at present employing the same linker register that supports red-light-inhibited gene
376 expression in *Dm*REDusk, we initially derived *Ac*PCM- and *Av*PCM-based systems giving rise to
377 constitutive target gene expression without pronounced light responses. Adjusting the length and
378 sequence of the linker intervening the PCM and the DHp/CA domains then yielded variants with
379 robust gene-expression responses to NIR light. Based on structural and biochemical evidence, said
380 linker is expected to form a continuous parallel α-helical coiled coil within the homodimeric SHK

381 (Bódizs et al., 2024; Burgie et al., 2024; Diensthuber et al., 2013; Jacob-Dubuisson et al., 2018; Malla
382 et al., 2024; Möglich, 2019; Möglich et al., 2009). Although other BphP-based photoreceptor designs
383 may involve linkers adopting different structures, the variation and probing of length and sequence
384 variants generally represents a worthwhile strategy that may eventually bear fruit. As, depending on
385 the use case, sizeable variant libraries may have to be assessed, two principal aspects emerge that
386 benefit the implementation of this strategy. First, the construction of libraries covering the desired
387 diversity in linker composition should be efficient, which can, e.g., be achieved by resorting to the
388 PATCHY protocol (Ohlendorf et al., 2016) as done here. Second, the screening for light-regulated
389 function should afford sufficient throughput, e.g., by coupling photoreceptor function to a
390 fluorescent readout or cell survival.

391 **Tunability of NIR-Light-Activated Two-Component Systems**

392 The recombination of bathy-BphP PCMs with a SHK effector module led to the pNIRusk plasmids for
393 stringent activation by NIR light of bacterial gene expression. As the underlying PCMs absorb light
394 over the entire near-UV to NIR region of the electromagnetic spectrum, the pNIRusk systems are
395 expected to also activate when exposed to other light colors. To dampen the commonly undesirable
396 activation by visible light and thereby facilitate the multiplexing with other photoresponsive circuits,
397 we deliberately chose *Ac*PCM and *Av*PCM because of their comparatively fast Pr→Pfr thermal
398 recovery. At photostationary state under constant illumination, a faster recovery results in an
399 effective desensitization against light, be it of blue, red, or NIR color (Ziegler and Möglich, 2015).
400 Consistent with this design rationale, the *Ac*NIRusk and *Av*NIRusk setups indeed exhibit half-maximal
401 light doses around ten times higher than for, e.g., *Dm*DERusk which relies on a conventional BphP
402 PCM (Meier et al., 2024a). Given its low phototoxicity, NIR light may be applied at even high powers
403 without harming the biological system under study. We note that NIR light around 800 nm is

404 commonly used in a therapeutic setting for photobiomodulation at intensities exceeding the ones
405 presently used by up to several orders of magnitude (Hamblin, 2016).

406 Perplexingly, the *Ac*NIRusk and *Av*NIRusk circuits respond moderately or very weakly to blue
407 and red light, respectively (see Fig. 2d, e). Although the strength of the gene-expression response
408 monotonically increases with the extent of Pfr→Pr photoconversion elicited by the individual light
409 colors within the underlying PCMs (see Fig. 1a-c), there is no direct proportionality. For instance,
410 *Ac*PCM roughly assumes a 0.7:0.3 photostationary Pr:Pfr equilibrium under red light (see Fig. 1a),
411 but at the level of gene expression, the response of the *Ac*NIRusk circuit to red light is only 2% that
412 of the NIR-light response. Initially unexpected, this baffling effect therefore further benefits the
413 application of the pNIRusk circuits in combination with other light-responsive entities, be it
414 optogenetic circuits or fluorescent reporters (Meier et al., 2024b; Tabor et al., 2011).

415 Our work provides pointers to the potential molecular underpinnings in that we isolated
416 additional pNIRusk variants with similar NIR-light responses but substantially higher expression
417 under red light (see Fig. 2b). Notably, these variants only differ in the composition of their linkers
418 connecting PCM to effector. Informed by our recent investigation of linker variants that culminated
419 in the generation of *Dm*DERusk (Meier et al., 2024a), we hypothesize that the different red-light
420 responses find their origin in an altered balance between the counteracting elementary histidine
421 kinase and phosphatase activities of SHKs. At the ensemble level, even small perturbations, e.g.,
422 caused by linker variation or changes in the Pr:Pfr proportion, can utterly tilt the net activity in either
423 the kinase or phosphatase direction (Landry et al., 2018; Möglich, 2019; Möglich et al., 2009; Russo
424 and Silhavy, 1993). The histidine kinase-phosphatase duality of TCSs thus provides a means of
425 rendering the signal response to light highly malleable and adaptable. At a practical level, when
426 engineering light-responsive TCSs, we advise to screen multiple candidate variants that may well
427 differ substantially in their signal response. As noted previously (Meier et al., 2024a), similar
428 concepts may also operate for cyclases (GGDEF) and phosphodiesterases (EAL) enzymes that

429 frequently occur in conjunction with BphP PCMs (Gourinchas et al., 2017) and that antagonistically
430 catalyze the making and breaking, respectively, of the bacterial second messenger cyclic-di-
431 guanosine monophosphate (Jenal et al., 2017).

432 **Applications in the NIR Future**

433 The advent of stringently controlled NIR-responsive bacterial gene-expression platforms now
434 facilitates a number of innovative applications. First, the currently available optogenetic setups for
435 expression regulation in bacteria predominantly respond to blue and red light but are often blind to
436 NIR light (Ohlendorf and Möglich, 2022). Given their fully intended relative insensitivity and their
437 unexpectedly weak response to visible light, the pNIRusk systems lend themselves to combinations
438 with pertinent setups. For example, applied at low to moderate intensity, blue light would trigger
439 one setup, e.g., pAurora2 or EL222-based systems (Jayaraman et al., 2016; Ranzani et al., 2024), but
440 leave pNIRusk largely untouched. By contrast, NIR light would selectively activate pNIRusk as the
441 LOV receptors underlying the blue-light-responsive setups are insensitive to this light quality. To
442 facilitate multiplexed applications of pNIRusk, we supply derivatives reliant on alternative TCSs that
443 can be readily combined in single bacterial cells and mediate the expression of several target genes
444 orchestrated by two light colors.

445 Second, NIR light penetrates mammalian tissue much more deeply than light of shorter
446 wavelengths (Lehtinen et al., 2022; Weissleder, 2001). This opens up intriguing applications involving
447 programmable, light-responsive bacteria as agents inside the bodies of mammals, e.g., as living
448 therapeutics (Cubillos-Ruiz et al., 2021; Hartsough et al., 2020). The pDawn system has already been
449 applied in this capacity within probiotic bacteria, but the approach has been hampered by delivering
450 blue light *in situ* (Cui et al., 2021; Magaraci et al., 2016; Pan et al., 2021; Sankaran and del Campo,
451 2019; Yang et al., 2020). One remedy has been the use of upconverting nanoparticles (UCNP)
452 administered alongside the light-responsive bacteria (Pan et al., 2021; Yang et al., 2020). Notably,

453 the UCNPs can be charged by absorption of several photons in the NIR range to then emit a photon
454 in the blue spectral region. Though feasible, pertinent applications introduce complexity and depart
455 from a purely genetically encoded optogenetic strategy. The new pNIRusk setups directly address
456 this challenge as they can be activated by essentially the same wavelengths previously used for
457 charging the UCNPs. Towards this goal, we demonstrate at present that both *Ac*NIRusk and *Av*NIRusk
458 operate in the probiotic *E. coli* Nissle strain out of the box, without need for optimization. Used in
459 place of pDawn, the pNIRusk systems thus obviate the need for the UCNPs and thereby broaden the
460 application scope of living therapeutics considerably.

461 Third, we demonstrate functionality of pNIRusk and pREDusk in the biotechnologically
462 relevant *A. tumefaciens* (Fig. 4c-d) which is widely used as a transfection vehicle in plant
463 biotechnology (Liu et al., 2013). Prospectively, both pNIRusk and pREDusk may achieve
464 spatiotemporal control of *A. tumefaciens* infectivity, e.g., to confine plant transfection to specific
465 time windows or organs. Of particular advantage, the bathochromically shifted absorbance spectra
466 of BphPs compared to plant Phys (Hughes and Winkler, 2024; Yi et al., 2025) stand to enable NIR-
467 light control without interfering with plant photoreception and photoautotrophic growth.

468 **Methods**

469 **Molecular Biology**

470 Oligonucleotides and plasmids used in this study are listed in Suppl. Tables 1 and 2. All plasmid
471 constructs were confirmed by Sanger sequencing (Microsynth Seqlab, Göttingen, Germany). To
472 produce bathy-BphP PCMs, the respective genes were introduced into a pCDF-Duet plasmid
473 (Novagen) already containing heme oxygenase 1 (HO1) from *Synechocystis* sp. for biliverdin supply
474 (Mukougawa et al., 2006; Stüven et al., 2019). To this end, the genes encoding the PCMs from *A.*
475 *caulinodans* (Uniprot A8HU76, residues 1-501), *A. vitis* (Uniprot B9JR96, residues 1-499), and *P.*

476 *aeruginosa* (Uniprot Q9HWR3, residues 1-497) were amplified by PCR from the template plasmids
477 pQX091, pQX086, and pQX037, respectively (Xu et al., 2024), followed by Gibson assembly (Gibson
478 et al., 2009).

479 The initial *Ac*NIRusk and *Av*NIRusk constructs (denoted '0') were created by exchanging
480 *Dm*PCM in *Dm*REDusk (Meier et al., 2024a) for *Ac*PCM and *Av*PCM, respectively (Suppl. Fig. 2), via
481 PCR amplification and Gibson assembly. The second amino acid in *Ac*PCM and *Av*PCM was changed
482 from proline to threonine to maintain the polycistronic structure of the operon comprising HO1, the
483 BphP-SHK, and the RR FixJ. To apply the PATCHY strategy (Ohlendorf et al., 2016), start constructs
484 were generated by elongating the PCM-DHp/CA linkers in the initial *Ac*NIRusk and *Av*NIRusk plasmids
485 as reported before (Meier et al., 2024a). The resulting constructs thus comprise the N-terminal
486 portions of the parental BphPs from A. *caulinodans* (Uniprot A8HU76) and *A. vitis* (Uniprot B9JR96)
487 up to and including residues 520 and 518, respectively, connected to the C-terminal fragment of *B.*
488 *japonicum* FixL starting from residue 257 (Uniprot P23222). At the junction, a restriction site for
489 *Ksp*AI and a one-nucleotide frameshift were inserted (Suppl. Fig. 3). Cloning was performed by two
490 consecutive overhang-PCRs and blunt-end ligation.

491 The TtrSR TCS from *Shewanella baltica* was introduced into *Dm*REDusk (Meier et al., 2024a)
492 by first replacing the FixK2 promoter by the 85-bp minimal promoter sequence PttrB185-269
493 (Daeffler et al., 2017) via PCR amplification and restriction cloning using *Bgl*II and *Xba*I sites. Next,
494 the *B. japonicum* FixLJ TCS was exchanged for the *S. baltica* TtrSR (Genbank CP000891.1, loci
495 Sbal195_3858 and Sbal195_3859) via Gibson assembly using as a PCR template a synthetic gene
496 (Gene Art) with codons optimized for expression in *E. coli*. For conducting PATCHY, a start construct
497 was made that includes residues 1-539 of the *Dm*BphP (Uniprot E8U3T3) and the *S. baltica* TtrSR
498 TCS (Uniprot A9L3S5) starting at residue 407. Cloning was performed as described above except that
499 an *Eco*32I restriction site and a two-nucleotide frameshift were placed at the junction between the
500 two gene fragments (Suppl. Fig. 6a).

501 The cognate TodX promoter of the TodST TCS from *Pseudomonas putida* was amplified by
502 PCR from pMIR77 (Ramos-González et al., 2002) and inserted into pDusk (Ohlendorf et al., 2012) by
503 restriction cloning with *Bgl*II and *Xba*I. Next, the TodST TCS was amplified from pMIR66 (Ramos-
504 González et al., 2002) and fused to the *Bacillus subtilis* YtvA LOV domain within pDusk via Gibson
505 cloning. The *Av*Tod-NIRusk PATCHY start construct was obtained by replacing YtvA-LOV with HO1 and
506 and *Av*PCM (residues 1-518) via Gibson assembly. The resultant construct comprised the TodS
507 starting from residue 726 (Uniprot E0X9C7) and TodT. At the junction, a *KspA*I restriction site and a
508 one-nucleotide frameshift were inserted (Suppl. Fig. 6b).

509 For multiplexing experiments, the *Ds*Red Express2 reporter gene (Strack et al., 2008) in
510 *Dm*DERusk and *Av*NIRusk was replaced by the YPet reporter gene (Nguyen and Daugherty, 2005).
511 Additionally, the kanamycin (Kan) resistance marker and the ColE1 origin of replication (ori) were
512 exchanged for streptomycin (Str) and a CloDF13 ori via Gibson assembly. A version of *Av*NIRusk
513 containing a multiple-cloning site rather than a fluorescent reporter was cloned by Gibson assembly
514 and deposited at Addgene for distribution (accession number 235084).

515 To apply *Dm*REDusk and *Av*NIRusk in *Agrobacterium tumefaciens*, the *Photorhabdus*
516 *luminescence luxABCDE* operon from pBAM2-luxAE (Dziuba et al., 2021) was cloned into the miniTn5
517 delivery plasmid pBAM2 (Uebe, unpublished). The sequence was amplified via PCR, digested with
518 *Nde*I/*Sac*I, and ligated into a similarly digested and Fast-AP-dephosphorylated pBAM2 vector to
519 generate pBAM2-luxAE. Subsequently, the light-regulated TCS cassettes of *Dm*REDusk (*DrhemO-*
520 *Dmpcm-fixL*) and *Av*NIRusk (*DrhemO-Avpcm-fixL*) were amplified. These genes were set under the
521 control of the strong constitutive *M. gryphiswaldense* PmamDC promoter. The *B. japonicum* FixK2
522 promoter was also amplified by PCR. The amplified fragments were fused by overlap extension PCR
523 and digested with *Nde*I/*Not*I as was the pBAM2-luxAE. Ligation resulted in the reporter plasmids
524 *Dm*REDlux and *Av*NIRlux in which the *luxABCDE* operon is under the control of the FixK2 promoter.

525 **Protein Purification**

526 For production of *Ac*PCM, *Av*PCM, and *Pa*PCM, *E. coli* LOBSTR cells (Andersen et al., 2013) were
527 transformed with the respective pCDF-Duet-PCM/HO1 constructs. Gene expression and protein
528 purification were performed as before (Meier et al., 2024a). Briefly, two flasks with 800 mL lysogeny
529 broth (LB) medium each supplemented with 100 µg mL^{-1} Str were inoculated with a 5-mL overnight
530 culture, and bacteria were grown in baffled Erlenmeyer flasks at 37°C and 225 rpm agitation. At an
531 optical density at 600 nm (OD_{600}) of around 0.7, the expression was induced by 1 mM isopropyl-β-
532 thiogalactopyranoside (IPTG), and 0.5 mM δ-aminolevulinic acid was added to support biliverdin
533 incorporation. The expression was performed at 16°C and 225 rpm agitation in darkness for around
534 65 h. All following steps were performed in green safe light. After harvesting the cells by
535 centrifugation, they were resuspended in lysis buffer [50 mM tris(hydroxy-methyl)-amino-methane
536 (Tris)/HCl, 20 mM NaCl, 10 mM imidazole, 1 mM β-mercaptoethanol, pH 8.0, protease inhibitor
537 completeOne (Roche), 1 mg mL^{-1} lysozyme]. Cells were lysed by sonification, and the supernatant of
538 the centrifuged lysate was applied to a HiTrap TALON crude column loaded with cobalt-
539 nitrilotriacetic resin (Cytiva). The column was washed with buffer [50 mM Tris/HCl, 20 mM NaCl, 1
540 mM β-mercaptoethanol, pH 8.0], and the His-tagged proteins were eluted by an imidazole gradient
541 from 0 to 0.5 M. Fractions were analyzed by denaturing SDS polyacrylamide gel electrophoresis
542 (PAGE) in the presence of 1 mM Zn^{2+} to visualize biliverdin incorporation (Berkelman and Lagarias,
543 1986) and pooled based on protein content. During an overnight dialysis at 4°C into buffer [50 mM
544 Tris/HCl, 20 mM NaCl, 1 mM β-mercaptoethanol, pH 8.0], the His-tag was cleaved off by His_6-tagged
545 TEV protease. The sample was applied twice to a gravity-flow IMAC column with HisPur cobalt resin
546 (ThermoFisher) using the same buffers as before. Cleavage of the His-tag and protein purity were
547 analyzed by Zn-SDS-PAGE. Fractions were pooled, dialyzed overnight at 4°C against storage buffer

548 [20 mM Tris/HCl, 20 mM NaCl, 10% (w/v) glycerol, 1 mM dithiothreitol, pH 8.0], concentrated via
549 spin filtration, and stored at -80°C.

550 **UV/vis Absorption Spectroscopy**

551 Absorption spectroscopy was carried out on a Cary60 UV/vis spectrophotometer (Agilent
552 Technologies) at 25°C under green safe light. Protein samples were diluted into buffers with pH
553 ranging from 6.0 to 11.0 (30 mM 2-(N-morpholino)ethanesulfonic acid/HCl, 30 mM NaCl, pH
554 6.0/6.5/7.0; 30 mM Tris/HCl, 30 mM NaCl, pH 7.5/8.0/8.5/9.0; 30 mM glycine/HCl, 30 mM NaCl, pH
555 10.0/10.5/11.0] (Rumfeldt et al., 2019). Samples were illuminated for 120 s with LEDs emitting in
556 the NIR [(800 ± 18) nm], red [(650 ± 10) nm] and blue [(470 ± 5) nm]. Data were normalized to the
557 Soret absorbance at 403 nm. Pr→Pfr dark recovery kinetics were monitored every 5 s at 760 nm and
558 fitted to single-exponential functions using the Fit-o-mat software (Möglich, 2018). Pr:Pfr ratios after
559 red or blue illumination were calculated via linear combination of the basis spectra as described
560 previously (Yi et al., 2025). The variation of photochemical parameters with pH was evaluated by
561 fitting to the Henderson-Hasselbalch equation. The ratio of the quantum yields Φ_p and Φ_q for the
562 red-light-driven photoconversion in the Pr→Pfr and Pfr→Pr directions, respectively (see Suppl. Fig.
563 1f), can be determined as follows (Yi et al., 2025):

564 $$\Phi_q/\Phi_p = P_R/P_{FR} \times (1 - 10^{-A_{Pr}})/(1 - 10^{-A_{Pfr}})$$

565 P_R and P_{FR} are the Pr and Pfr proportions at red-light-induced photostationary state, and A_{Pr} and A_{Pfr}
566 denote the absorbance in the Pr and Pfr states at the peak emission wavelength of the red-light
567 source.

568 **Generation and Screening of Linker Variants**

569 *Ac*NIRusk, *Av*NIRusk, *Dm*Ttr-REDusk and *Av*Tod-NIRusk linker variants were created with the PATCHY
570 strategy (Meier et al., 2024a; Ohlendorf et al., 2016). Sets of forward and reverse primers to generate

571 linker variants were designed using a custom Python script (https://github.com/vrylr/PATCHY). In
572 brief, PCR amplification was carried out using the primer sets in a final concentration of 0.25 µM.
573 After purifying the PCR product by gel extraction, the start constructs were digested with *Ksp*AI or
574 *Eco*32I (Suppl. Fig. 3, 6), followed by phosphorylation with T4 polynucleotide kinase and ligation with
575 T4 DNA ligase. The reaction mixes were transformed into DH10b cells and plated on LB plates
576 supplemented with kanamycin (LB/Kan). Plates were incubated overnight at 37°C in darkness, or
577 under red light [100 µW cm^{-2}, (650 ± 11) nm] or NIR light [200 µW cm^{-2}, (800 ± 18) nm]. Applied light
578 intensities were calibrated with a power meter (model 842-PE, equipped with a 918D-UV-OD3 silicon
579 photodiode, Newport, Darmstadt, Germany). Bacterial colonies developing red color upon overnight
580 incubation, indicative of *Ds*Red production, were used to inoculate 200 µL LB/Kan in a clear 96-well
581 microtiter plate (MTP) (Nunc, ThermoFisher). Bacteria were incubated for 21-24 h at 30°C and 750
582 rpm agitation. Next, the cultures were diluted 100-fold into fresh LB/Kan medium and split into three
583 separate cultures which were then incubated at 37°C and 750 rpm agitation in either darkness, red
584 light [100 µW cm^{-2}, (650 ± 11) nm], or NIR light [200 µW cm^{-2}, (800 ± 18) nm]. After 18 h, the optical
585 density at (600 ± 9) nm (OD_{600}) and the *Ds*Red fluorescence [(554 ± 9) nm excitation and (591 ± 20)
586 nm emission] were measured with a Tecan Infinite M200 Pro MTP reader (Tecan Group, Ltd.,
587 Männedorf, Switzerland). The *Ds*Red fluorescence was normalized to OD_{600} and represent the mean
588 ± s.d. of three biologically independent replicates.

589 **Light-Dose-Response Assays in *Escherichia coli***

590 Analyses were performed as before (Meier et al., 2024a; Multamäki et al., 2022). *E. coli* CmpX13 or
591 *E. coli* Nissle (*Ec*N, DSMZ no. 115365) bacteria containing the respective construct were used to
592 inoculate 5 mL LB medium supplemented with 50 µg mL^{-1} Kan or 100 µg mL^{-1} Str (LB/Str). Cultures
593 were incubated for 21-24 h at 30°C and 225 rpm agitation under non-inducing light conditions.
594 Under green safe light, the bacteria were diluted 100-fold into fresh LB/Kan or LB/Str, before

595 distributing 200 µL each into 64 wells of a black-walled MTP with clear bottom (µClear, Greiner
596 BioOne, Frickenhausen, Germany). As a control, bacteria harboring an MCS variant were also placed
597 on the MTP. After sealing the MTP with a gas-permeable membrane, it was placed on an Arduino-
598 controlled illumination device. For the application of red and blue light, a previous setup was used
599 (Hennemann et al., 2018) with LED peak wavelengths of (624 ± 8) nm and (463 ± 12) nm, respectively.
600 To apply NIR light, we devised a new matrix of 8-by-8 LEDs emitting at (800 ± 18) nm (LED800-01AU,
601 Roithner Lasertechnik) which is controlled by an Arduino circuit board (Suppl. Fig. 4). The bacteria
602 inside the MTPs were incubated for 18 h at 37°C and 750 rpm agitation. The illumination was applied
603 in 1:2 or 1:10 duty cycles (i.e., 1 s light and 1 s darkness, or 20 s light and 180 s darkness). After
604 incubation, the OD_{600} and *Ds*Red fluorescence were determined as above. For measurements of YPet
605 fluorescence, excitation and emission wavelengths of (500 ± 9) nm and (554 ± 9) nm were used.
606 Following normalization to OD_{600}, the MCS background was subtracted. Data represent mean ± s.d.
607 of three biological replicates and were evaluated as a function of the light intensity averaged over
608 the duty cycle according to Hill isotherms using Fit-o-mat.

609 **Flow Cytometry**

610 *E. coli* CmpX13 cells (Mathes et al., 2009) containing *Ac*NIRusk, *Av*NIRusk, or an empty-vector control
611 (MCS) were analyzed by flow cytometry (Meier et al., 2024a). After overnight incubation for 21-24
612 h at 30°C and 750 rpm agitation, bacterial cultures were diluted 100-fold into fresh LB/Kan medium.
613 For each variant, the cultures were split in three and incubated for 18 h at 37°C and 750 rpm agitation
614 in either darkness, red light [100 µW cm^{-2}, (650 ± 11) nm], or different intensities (18-270 µW cm^{-2})
615 of NIR light [(800 ± 18) nm]. Following incubation, the cultures were diluted 10-fold into phosphate-
616 buffered saline (1x sheath fluid, Bio-Rad) and analyzed on a S3e cell sorter (Bio-Rad). The *Ds*Red
617 fluorescence of at least 200,000 events was detected using excitation lasers at 488 nm and 561 nm

618 and an emission channel at (585 ± 15) nm. Data were fitted to skewed Gaussian distributions using
619 Fit-o-mat. Experiments were repeated three times with similar results.

620 **Multiplexing of Optogenetic Circuits**

621 Pairs of plasmids harboring light-responsive TCSs were serially transformed into chemically
622 competent *E. coli* CmpX13. 200 µL LB supplemented with 50 µg mL^{-1} Kan and 100 µg mL^{-1} Str
623 (LB/Kan+Str) were inoculated with single bacterial clones and incubated for 21-24 h inside MTP wells
624 at 30°C and 750 rpm agitation in darkness. The cultures were then diluted 100-fold into LB/Kan+Str
625 before dispensation of 200 µL each into individual wells of four µClear MTPs. The MTPs were
626 incubated for 18 h at 37°C and 750 rpm agitation in either darkness, under red light [100 µW cm^{-2},
627 (624 ± 8) nm], NIR light [200 µW cm^{-2}, (800 ± 18) nm], or both light colors combined. Where
628 applicable, red light was applied continuously from below using the Arduino-controlled RGB LED
629 matrix, whereas NIR light shone from above. After 18 h incubation, the OD_{600}, and *Ds*Red and YPet
630 fluorescence were measured as above. Data were normalized to the maximal *Ds*Red and YPet
631 readings and represent mean ± s.d. of three biological replicates.

632 **Luciferase Assays in *Agrobacterium tumefaciens***

633 The *Dm*REDlux and *Av*NIRlux plasmids were transferred to *Agrobacterium tumefaciens* C58 (also
634 known as *Agrobacterium fabrum* C58, Lab collection, ATCC 33970) by biparental conjugation using
635 *E. coli* WM3064 as a diaminopimelic acid auxotrophic donor strain (William Metcalf, UIUC,
636 unpublished; *thrB1004 pro thi rpsL hsdS lacZ*Δ*M15* RP4-1360 *Δ(araBAD)567 ΔdapA1341::[erm pir*
637 *(wt)])*. Unless specified otherwise, C58 was routinely cultivated in LB medium at 28°C with 170 rpm
638 agitation. Selection for mini-Tn5 insertion mutants carrying the *lux* reporter constructs was carried
639 out on solid LB with 1.5% (w/v) agar and 50 µg mL^{-1} Kan. *E. coli* WM3064 strains carrying plasmids

640 were cultivated at 37°C with 200 rpm shaking in LB supplemented with 0.1 mM DL-a,e-
641 diaminopimelic acid (DAP) and 25 µg mL^{-1} Kan or 50 µg mL^{-1} ampicillin (Amp).

642 The protocol for biparental conjugation was described before (Dziuba et al., 2021). Briefly,
643 cultures of the C58 receptor and plasmid-containing *E. coli* strains were cultivated in LB or LB/Amp
644 medium overnight. Then, 2×10^9 cells of each strain were mixed in 15-mL falcon tubes and pelleted
645 at 5,421 g for 10 min. The supernatant was discarded while the cell pellet was resuspended in 100-
646 200 µL LB medium and spotted onto LB agar plates. After overnight incubation at 28°C, cells were
647 resuspended in 1 mL LB and transferred to 15-mL falcon tubes containing 9 mL LB medium. After
648 incubation for 2 h at 28°C and 120 rpm agitation, the cell suspension was pelleted by centrifugation,
649 and the supernatant was discarded. Following resuspension in 1 mL LB medium, 100 µL of 10- and
650 100-fold diluted cell suspensions were plated on LB-Kan agar plates. After incubation for three days
651 at 28°C, Kan-resistance plasmid insertion mutants were transferred to fresh LB/Kan agar plates and
652 screened by PCR.

653 At least three randomly selected transconjugants containing the luciferase reporter
654 constructs were analyzed for luminescence. Each experiment was performed in duplicate.
655 Luminescence signals, measured as arbitrary light units (ALU), were detected using a Tecan Infinite
656 M200 Pro MTP reader equipped with a luminometer module (Tecan Group, Ltd., Männedorf,
657 Switzerland) during culture growth in LB medium at 23°C and 280 rpm. Measurements were taken
658 every 20 minutes over 300 cycles (~90 h). ALU readings were normalized to the optical density at
659 650 nm (OD_{650}) to calculate the relative light units (RLU). To this end, tested clones were inoculated
660 into 600 µL LB/Kan medium in 24-well plates and incubated for ~ 20 h under non-inducing conditions
661 (i.e., red light for *Dm*REDlux and darkness for *Av*NIRlux, respectively) at 28°C and 140 rpm. Cultures
662 were then diluted 10-fold into 1 mL LB/Kan and incubated under identical conditions for an
663 additional 4-5 h. Subsequently, the OD_{650} was adjusted to 0.1 by adding fresh LB/Kan medium, and
664 100 µL of the normalized cell suspension was transferred into two 96-well MTPs. Cultivation of both

665 MTPs was initiated simultaneously, with one incubated under dark conditions and the other one
666 under red [(650 ± 11) nm] or NIR light [(800 ± 18) nm].

667 Alternatively, luminescence was assessed using a spotting assay. Precultures were prepared
668 as above, and 5 µL of the OD_{650}-normalized cell suspension were spotted onto LB/Kan agar plates.
669 The plates were incubated for 44 h at 28°C under dark conditions or under blue [(470 ± 13) nm], red
670 [(650 ± 11) nm], or NIR light [(800 ± 18) nm]. Luminescence signals were documented as cumulative
671 signal intensities using the Bio-Rad ChemiDoc XRS+ System (Bio Rad Laboratories Inc., Herkules,
672 USA), with images captured every 0.6 s over a 1-min period. In addition, colorimetric images were
673 acquired to visualize the outlines of the spotted cell suspensions. Luminescence was quantified from
674 the image time series by calculating the slope of the mean pixel intensities within the outlined cell
675 suspension areas using the Image J Fiji package (v1.54f) (Schindelin et al., 2012). Background
676 correction was performed by subtracting the mean pixel intensity of an uninoculated region of the
677 agar plate.

678 **References**

679 Abramson J, Adler J, Dunger J, Evans R, Green T, Pritzel A, Ronneberger O, Willmore L, Ballard AJ, Bambrick J,
680 Bodenstein SW, Evans DA, Hung C-C, O'Neill M, Reiman D, Tunyasuvunakool K, Wu Z, Žemgulytė A,
681 Arvaniti E, Beattie C, Bertolli O, Bridgland A, Cherepanov A, Congreve M, Cowen-Rivers AI, Cowie A,
682 Figurnov M, Fuchs FB, Gladman H, Jain R, Khan YA, Low CMR, Perlin K, Potapenko A, Savy P, Singh S,
683 Stecula A, Thillaisundaram A, Tong C, Yakneen S, Zhong ED, Zielinski M, Žídek A, Bapst V, Kohli P, Jaderberg
684 M, Hassabis D, Jumper JM. 2024. Accurate structure prediction of biomolecular interactions with
685 AlphaFold 3. *Nature* **630**:493–500. doi:10.1038/s41586-024-07487-w

686 Andersen KR, Leksa NC, Schwartz TU. 2013. Optimized E. coli expression strain LOBSTR eliminates common
687 contaminants from His-tag purification. *Prot Struct Funct Bioinf* **81**:1857–1861. doi:10.1002/prot.24364

688 Anthamatten D, Hennecke H. 1991. The regulatory status of the fixL- and fixJ-like genes in Bradyrhizobium
689 japonicum may be different from that in Rhizobium meliloti. *Mol Gen Genet* **225**:38–48.

690 Ash C, Dubec M, Donne K, Bashford T. 2017. Effect of wavelength and beam width on penetration in light-
691 tissue interaction using computational methods. *Lasers Med Sci* **32**:1909–1918. doi:10.1007/s10103-017-
692 2317-4

693 Berkelman TR, Lagarias JC. 1986. Visualization of bilin-linked peptides and proteins in polyacrylamide gels.
694 *Anal Biochem* **156**:194–201.

695 Blum M, Andreeva A, Florentino LC, Chuguransky SR, Grego T, Hobbs E, Pinto BL, Orr A, Paysan-Lafosse T,
696 Ponamareva I, Salazar GA, Bordin N, Bork P, Bridge A, Colwell L, Gough J, Haft DH, Letunic I, Llinares-López
697 F, Marchler-Bauer A, Meng-Papaxanthos L, Mi H, Natale DA, Orengo CA, Pandurangan AP, Piovesan D,
698 Rivoire C, Sigrist CJA, Thanki N, Thibaud-Nissen F, Thomas PD, Tosatto SCE, Wu CH, Bateman A. 2025.
699 InterPro: the protein sequence classification resource in 2025. *Nucl Acids Res* **53**:D444–D456.
700 doi:10.1093/nar/gkae1082

701 Bódizs S, Mészáros P, Grunewald L, Takala H, Westenhoff S. 2024. Cryo-EM structures of a bathy phytochrome
702 histidine kinase reveal a unique light-dependent activation mechanism. *Structure* **32**:1952-1962.e3.
703 doi:10.1016/j.str.2024.08.008

704 Böhm C, Lehtinen K, Multamäki E, Vanhatalo R, Brander O, Meier SSM, Rumfeldt JA, Möglich A, Takala H.
705 2025. Traits and application of bathy phytochromes to bacterial optogenetics. *submitted*.

706 Borucki B, von Stetten D, Seibeck S, Lamparter T, Michael N, Mroginski MA, Otto H, Murgida DH, Heyn MP,
707 Hildebrandt P. 2005. Light-induced proton release of phytochrome is coupled to the transient
708 deprotonation of the tetrapyrrole chromophore. *J Biol Chem* **280**:34358–64.

709 Burgie ES, Basore K, Rau MJ, Summers B, Mickles AJ, Grigura V, Fitzpatrick JAJ, Vierstra RD. 2024. Signaling by
710 a bacterial phytochrome histidine kinase involves a conformational cascade reorganizing the dimeric
711 photoreceptor. *Nat Commun* **15**:6853. doi:10.1038/s41467-024-50412-y

712 Busch A, Guazzaroni M-E, Lacal J, Ramos JL, Krell T. 2009. The Sensor Kinase TodS Operates by a Multiple Step
713 Phosphorelay Mechanism Involving Two Autokinase Domains*. *J Biol Chem* **284**:10353–10360.
714 doi:10.1074/jbc.M900521200

715 Buschiazzo A, Trajtenberg F. 2019. Two-Component Sensing and Regulation: How Do Histidine Kinases Talk
716 with Response Regulators at the Molecular Level? *Annu Rev Micro* **73**:507–528. doi:10.1146/annurev-
717 micro-091018-054627

718 Chernov KG, Redchuk TA, Omelina ES, Verkhusha VV. 2017. Near-Infrared Fluorescent Proteins, Biosensors,
719 and Optogenetic Tools Engineered from Phytochromes. *Chem Rev* **117**:6423–6446.
720 doi:10.1021/acs.chemrev.6b00700

721 Cubillos-Ruiz A, Guo T, Sokolovska A, Miller PF, Collins JJ, Lu TK, Lora JM. 2021. Engineering living therapeutics
722 with synthetic biology. *Nat Rev Drug Discov* **20**:941–960. doi:10.1038/s41573-021-00285-3

723 Cui M, Sun T, Li Shubin, Pan H, Liu J, Zhang X, Li L, Li Shanshan, Wei C, Yu C, Yang C, Ma N, Ma B, Lu S, Chang
724 J, Zhang W, Wang H. 2021. NIR light-responsive bacteria with live bio-glue coatings for precise
725 colonization in the gut. *Cell Rep* **36**:109690. doi:10.1016/j.celrep.2021.109690

726 Daeffler KN, Galley JD, Sheth RU, Ortiz-Velez LC, Bibb CO, Shroyer NF, Britton RA, Tabor JJ. 2017. Engineering
727 bacterial thiosulfate and tetrathionate sensors for detecting gut inflammation. *Mol Syst Biol* **13**:923.
728 doi:10.15252/msb.20167416

729 Davis SJ, Vener AV, Vierstra RD. 1999. Bacteriophytochromes: Phytochrome-Like Photoreceptors from
730 Nonphotosynthetic Eubacteria. *Science* **286**:2517–2520. doi:10.1126/science.286.5449.2517

731 Deisseroth K, Feng G, Majewska AK, Miesenböck G, Ting A, Schnitzer MJ. 2006. Next-generation optical
732 technologies for illuminating genetically targeted brain circuits. *J Neurosci* **26**:10380–10386.
733 doi:10.1523/JNEUROSCI.3863-06.2006

734 Diensthuber RP, Bommer M, Gleichmann T, Möglich A. 2013. Full-length structure of a sensor histidine kinase
735 pinpoints coaxial coiled coils as signal transducers and modulators. *Structure* **21**:1127–1136.
736 doi:10.1016/j.str.2013.04.024

737 Dziuba M, Riese CN, Borgert L, Wittchen M, Busche T, Kalinowski J, Uebe R, Schüler D. 2021. The Complex
738 Transcriptional Landscape of Magnetosome Gene Clusters in Magnetospirillum gryphiswaldense.
739 *mSystems* **6**:10.1128/msystems.00893-21. doi:10.1128/msystems.00893-21

740 Etzl S, Lindner R, Nelson MD, Winkler A. 2018. Structure-guided design and functional characterization of an
741 artificial red light–regulated guanylate/adenylate cyclase for optogenetic applications. *J Biol Chem*
742 **293**:9078–9089. doi:10.1074/jbc.RA118.003069

743 Gao R, Bouillet S, Stock AM. 2019. Structural Basis of Response Regulator Function. *Annu Rev Micro* **73**:175–
744 197. doi:10.1146/annurev-micro-020518-115931

745 Gibson DG, Young L, Chuang R-Y, Venter JC, Hutchison CA, Smith HO. 2009. Enzymatic assembly of DNA
746 molecules up to several hundred kilobases. *Nat Methods* **6**:343–345. doi:10.1038/nmeth.1318

747 Gourinchas G, Etzl S, Göbl C, Vide U, Madl T, Winkler A. 2017. Long-range allosteric signaling in red light-
748 regulated diguanylyl cyclases. *Sci Adv* **3**:e1602498. doi:10.1126/sciadv.1602498

749 Hamblin MR. 2016. Shining light on the head: Photobiomodulation for brain disorders. *BBA Clinical* **6**:113–
750 124. doi:10.1016/j.bbacli.2016.09.002

751 Hartsough LA, Park M, Kotlajich MV, Lazar JT, Han B, Lin C-CJ, Musteata E, Gambill L, Wang MC, Tabor JJ. 2020.
752 Optogenetic control of gut bacterial metabolism to promote longevity. *Elife* **9**:e56849.
753 doi:10.7554/eLife.56849

754 Hennemann J, Iwasaki RS, Grund TN, Diensthuber RP, Richter F, Möglich A. 2018. Optogenetic Control by
755 Pulsed Illumination. *Chembiochem* **19**:1296–1304. doi:10.1002/cbic.201800030

756 Huber C, Strack M, Schultheiß I, Pielage J, Mechler X, Hornbogen J, Diller R, Frankenberg-Dinkel N. 2024.
757 Darkness inhibits autokinase activity of bacterial bathy phytochromes. *J Biol Chem* **300**:107148.
758 doi:10.1016/j.jbc.2024.107148

759 Hughes J, Lamparter T, Mittmann F, Hartmann E, Gärtner W, Wilde A, Börner T. 1997. A prokaryotic
760 phytochrome. *Nature* **386**:663. doi:10.1038/386663a0

761 Hughes J, Winkler A. 2024. New Insight Into Phytochromes: Connecting Structure to Function. *Annu Rev Plant*
762 *Biol* **75**:153–183. doi:10.1146/annurev-arplant-070623-110636

763 Jacob-Dubuisson F, Mechaly A, Betton J-M, Antoine R. 2018. Structural insights into the signalling mechanisms
764 of two-component systems. *Nat Rev Micro* **16**:585. doi:10.1038/s41579-018-0055-7

765 Jayaraman P, Devarajan K, Chua TK, Zhang H, Gunawan E, Poh CL. 2016. Blue light-mediated transcriptional
766 activation and repression of gene expression in bacteria. *Nucl Acids Res* **44**:6994–7005.
767 doi:10.1093/nar/gkw548

768 Jenal U, Reinders A, Lori C. 2017. Cyclic di-GMP: second messenger extraordinaire. *Nat Rev Microbiol* **15**:271–
769 284. doi:10.1038/nrmicro.2016.190

770 Karniol B, Vierstra RD. 2003. The pair of bacteriophytochromes from Agrobacterium tumefaciens are histidine
771 kinases with opposing photobiological properties. *Proc Natl Acad Sci U S A* **100**:2807–2812.
772 doi:10.1073/pnas.0437914100

773 Krell T, Lacal J, Busch A, Silva-Jiménez H, Guazzaroni M-E, Ramos JL. 2010. Bacterial Sensor Kinases: Diversity
774 in the Recognition of Environmental Signals. *Annu Rev Micro* **64**:539–559.
775 doi:10.1146/annurev.micro.112408.134054

776 Lamparter T, Michael N, Mittmann F, Esteban B. 2002. Phytochrome from Agrobacterium tumefaciens has
777 unusual spectral properties and reveals an N-terminal chromophore attachment site. *Proc Natl Acad Sci*
778 *U S A* **99**:11628–11633. doi:10.1073/pnas.152263999

779 Landry BP, Palanki R, Dyulgyarov N, Hartsough LA, Tabor JJ. 2018. Phosphatase activity tunes two-component
780 system sensor detection threshold. *Nat Commun* **9**:1433. doi:10.1038/s41467-018-03929-y

781 Lau PCK, Wang Y, Patel A, Labbé D, Bergeron H, Brousseau R, Konishi Y, Rawlings M. 1997. A bacterial basic
782 region leucine zipper histidine kinase regulating toluene degradation. *Proc Natl Acad Sci U S A* **94**:1453–
783 1458. doi:10.1073/pnas.94.4.1453

784 Laub MT, Goulian M. 2007. Specificity in Two-Component Signal Transduction Pathways. *Annu Rev Genet*
785 **41**:121–145. doi:10.1146/annurev.genet.41.042007.170548

786 Lazar JT, Tabor JJ. 2021. Bacterial two-component systems as sensors for synthetic biology applications. *Curr*
787 *Opin Syst Biol* **28**:100398. doi:10.1016/j.coisb.2021.100398

788 Lehtinen K, Nokia MS, Takala H. 2022. Red Light Optogenetics in Neuroscience. *Front Cell Neurosci* **15**.

789 Leopold AV, Chernov KG, Shemetov AA, Verkhusha VV. 2019. Neurotrophin receptor tyrosine kinases
790 regulated with near-infrared light. *Nat Commun* **10**:1–13. doi:10.1038/s41467-019-08988-3

791 Leopold AV, Thankachan S, Yang C, Gerashchenko D, Verkhusha VV. 2022. A general approach for engineering
792 RTKs optically controlled with far-red light. *Nat Methods* **19**:871–880. doi:10.1038/s41592-022-01517-z

793 Levskaya A, Chevalier AA, Tabor JJ, Simpson ZB, Lavery LA, Levy M, Davidson EA, Scouras A, Ellington AD,
794 Marcotte EM, Voigt CA. 2005. Synthetic biology: Engineering Escherichia coli to see light. *Nature*
795 **438**:441–442. doi:10.1038/nature04405

796 Liu W, Yuan JS, Stewart Jr CN. 2013. Advanced genetic tools for plant biotechnology. *Nat Rev Genet* **14**:781–
797 793. doi:10.1038/nrg3583

798 Magaraci MS, Bermudez JG, Yogish D, Pak DH, Mollov V, Tycko J, Issadore D, Mannickarottu SG, Chow BY. 2016.
799 Toolbox for Exploring Modular Gene Regulation in Synthetic Biology Training. *ACS Synth Biol* **5**:781–785.
800 doi:10.1021/acssynbio.6b00057

801 Malla TN, Hernandez C, Muniyappan S, Menendez D, Bizhga D, Mendez JH, Schwander P, Stojković EA, Schmidt
802 M. 2024. Photoreception and signaling in bacterial phytochrome revealed by single-particle cryo-EM. *Sci*
803 *Adv* **10**:eadq0653. doi:10.1126/sciadv.adq0653

804 Meier SSM, Multamäki E, Ranzani AT, Takala H, Möglich A. 2024a. Leveraging the histidine kinase-phosphatase
805 duality to sculpt two-component signaling. *Nat Commun* **15**:4876. doi:10.1038/s41467-024-49251-8

806 Meier SSM, Multamäki E, Ranzani AT, Takala H, Möglich A. 2024b. Multimodal Control of Bacterial Gene
807 Expression by Red and Blue Light. *Meth Mol Biol* **2760**:463–477. doi:10.1007/978-1-0716-3658-9_26

808 Möglich A. 2019. Signal transduction in photoreceptor histidine kinases. *Prot Sci* **28**:1923–1946.
809 doi:10.1002/pro.3705

810 Möglich A. 2018. An Open-Source, Cross-Platform Resource for Nonlinear Least-Squares Curve Fitting. *J Chem*
811 *Educ* **95**:2273–2278. doi:10.1021/acs.jchemed.8b00649

812 Möglich A, Ayers RA, Moffat K. 2010. Addition at the molecular level: signal integration in designed Per-ARNT-
813 Sim receptor proteins. *J Mol Biol* **400**:477–486. doi:10.1016/j.jmb.2010.05.019

814 Möglich A, Ayers RA, Moffat K. 2009. Design and signaling mechanism of light-regulated histidine kinases. *J*
815 *Mol Biol* **385**:1433–1444. doi:10.1016/j.jmb.2008.12.017

816 Mukougawa K, Kanamoto H, Kobayashi T, Yokota A, Kohchi T. 2006. Metabolic engineering to produce
817 phytochromes with phytochromobilin, phycocyanobilin, or phycoerythrobilin chromophore in
818 Escherichia coli. *FEBS Lett* **580**:1333–1338. doi:10.1016/j.febslet.2006.01.051

819 Multamäki E, García de Fuentes A, Sieryi O, Bykov A, Gerken U, Ranzani AT, Köhler J, Meglinski I, Möglich A,
820 Takala H. 2022. Optogenetic Control of Bacterial Expression by Red Light. *ACS Synth Biol* **11**:3354–3367.
821 doi:10.1021/acssynbio.2c00259

822 Multamäki E, Nanekar R, Morozov D, Lievonen T, Golonka D, Wahlgren WY, Stucki-Buchli B, Rossi J, Hytönen
823 VP, Westenhoff S, Ihalainen JA, Möglich A, Takala H. 2021. Comparative analysis of two paradigm
824 bacteriophytochromes reveals opposite functionalities in two-component signaling. *Nat Commun*
825 **12**:4394. doi:10.1038/s41467-021-24676-7

826 Nguyen AW, Daugherty PS. 2005. Evolutionary optimization of fluorescent proteins for intracellular FRET. *Nat*
827 *Biotechnol* **23**:355–360. doi:10.1038/nbt1066

828 Ohlendorf R, Möglich A. 2022. Light-regulated gene expression in Bacteria: Fundamentals, advances, and
829 perspectives. *Front Bioeng Biotech* **10**:1029403.

830 Ohlendorf R, Schumacher CH, Richter F, Möglich A. 2016. Library-Aided Probing of Linker Determinants in
831 Hybrid Photoreceptors. *ACS Synth Biol* **5**:1117–1126. doi:10.1021/acssynbio.6b00028

832 Ohlendorf R, Vidavski RR, Eldar A, Moffat K, Möglich A. 2012. From dusk till dawn: one-plasmid systems for
833 light-regulated gene expression. *J Mol Biol* **416**:534–542. doi:10.1016/j.jmb.2012.01.001

834 Ong NT, Olson EJ, Tabor JJ. 2018. Engineering an E. coli Near-Infrared Light Sensor. *ACS Synth Biol* **7**:240–248.
835 doi:10.1021/acssynbio.7b00289

836 Pan H, Li L, Pang G, Han C, Liu B, Zhang Y, Shen Y, Sun T, Liu J, Chang J, Wang H. 2021. Engineered NIR light-
837 responsive bacteria as anti-tumor agent for targeted and precise cancer therapy. *Chem Eng J* **426**:130842.
838 doi:10.1016/j.cej.2021.130842

839 Parkinson JS, Kofoid EC. 1992. Communication Modules in Bacterial Signaling Proteins. *Annu Rev Genet*
840 **26**:71–112. doi:10.1146/annurev.ge.26.120192.000443

841 Ramos-González M-I, Olson M, Gatenby AA, Mosqueda G, Manzanera M, Campos MJ, Víchez S, Ramos JL.
842 2002. Cross-Regulation between a Novel Two-Component Signal Transduction System for Catabolism of

843 Toluene in Pseudomonas mendocina and the TodST System from Pseudomonas putida. *J Bact* **184**:7062–
844 7067. doi:10.1128/jb.184.24.7062-7067.2002

845 Ranzani AT, Buchholz K, Blackholm M, Kopkin H, Möglich A. 2024. Induction of bacterial expression at the
846 mRNA level by light. *Nucl Acids Res* **52**:10017–10028. doi:10.1093/nar/gkae678

847 Rottwinkel G, Oberpichler I, Lamparter T. 2010. Bathy Phytochromes in Rhizobial Soil Bacteria. *J Bact*
848 **192**:5124–5133. doi:10.1128/JB.00672-10

849 Rumfeldt JA, Takala H, Liukkonen A, Ihalainen JA. 2019. UV-Vis Spectroscopy Reveals a Correlation Between
850 Y263 and BV Protonation States in Bacteriophytochromes. *Photochem Photobiol* **95**:969–979.
851 doi:https://doi.org/10.1111/php.13095

852 Russo FD, Silhavy TJ. 1993. The essential tension: opposed reactions in bacterial two-component regulatory
853 systems. *Trends Microbiol* **1**:306–310.

854 Sankaran S, del Campo A. 2019. Optoregulated Protein Release from an Engineered Living Material. *Adv*
855 *Biosyst* **3**:1800312. doi:10.1002/adbi.201800312

856 Schindelin J, Arganda-Carreras I, Frise E, Kaynig V, Longair M, Pietzsch T, Preibisch S, Rueden C, Saalfeld S,
857 Schmid B, Tinevez J-Y, White DJ, Hartenstein V, Eliceiri K, Tomancak P, Cardona A. 2012. Fiji: an open-
858 source platform for biological-image analysis. *Nat Methods* **9**:676–682. doi:10.1038/nmeth.2019

859 Schmidl SR, Sheth RU, Wu A, Tabor JJ. 2014. Refactoring and Optimization of Light-Switchable Escherichia coli
860 Two-Component Systems. *ACS Synth Biol* **3**:820–831. doi:10.1021/sb500273n

861 Schmidt A, Sauthof L, Szczepek M, Lopez MF, Escobar FV, Qureshi BM, Michael N, Buhrke D, Stevens T,
862 Kwiatkowski D, von Stetten D, Mroginski MA, Krauß N, Lamparter T, Hildebrandt P, Scheerer P. 2018.
863 Structural snapshot of a bacterial phytochrome in its functional intermediate state. *Nat Commun* **9**:4912.
864 doi:10.1038/s41467-018-07392-7

865 Silva-Jiménez H, Ramos JL, Krell T. 2012. Construction of a prototype two-component system from the
866 phosphorelay system TodS/TodT. *Protein Eng Des Sel* **25**:159–169. doi:10.1093/protein/gzs001

867 Stabel R, Stüven B, Hansen JN, Körschen HG, Wachten D, Möglich A. 2019. Revisiting and Redesigning Light-
868 Activated Cyclic-Mononucleotide Phosphodiesterases. *J Mol Biol* **431**:3029–3045.
869 doi:10.1016/j.jmb.2019.07.011

870 Strack RL, Strongin DE, Bhattacharyya D, Tao W, Berman A, Broxmeyer HE, Keenan RJ, Glick BS. 2008. A
871 noncytotoxic DsRed variant for whole-cell labeling. *Nat Methods* **5**:955–957. doi:10.1038/nmeth.1264

872 Stüven B, Stabel R, Ohlendorf R, Beck J, Schubert R, Möglich A. 2019. Characterization and engineering of
873 photoactivated adenylyl cyclases. *Biol Chem* **400**:429–441. doi:10.1515/hsz-2018-0375

874 Tabor JJ, Levskaya A, Voigt CA. 2011. Multichromatic control of gene expression in Escherichia coli. *J Mol Biol*
875 **405**:315–324. doi:10.1016/j.jmb.2010.10.038

876 Takala H, Edlund P, Ihalainen JA, Westenhoff S. 2020. Tips and turns of bacteriophytochrome photoactivation.
877 *Photochem Photobiol Sci* **19**:1488–1510. doi:10.1039/D0PP00117A

878 Tang K, Beyer HM, Zurbriggen MD, Gärtner W. 2021. The Red Edge: Bilin-Binding Photoreceptors as
879 Optogenetic Tools and Fluorescence Reporters. *Chem Rev* **121**:14906–14956.
880 doi:10.1021/acs.chemrev.1c00194

881 Tasler R, Moises T, Frankenberg-Dinkel N. 2005. Biochemical and spectroscopic characterization of the
882 bacterial phytochrome of Pseudomonas aeruginosa. *FEBS J* **272**:1927–1936. doi:10.1111/j.1742-
883 4658.2005.04623.x

884 Velazquez Escobar F, Piwowarski P, Salewski J, Michael N, Fernandez Lopez M, Rupp A, Qureshi BM, Scheerer
885 P, Bartl F, Frankenberg-Dinkel N, Siebert F, Andrea Mroginski M, Hildebrandt P. 2015. A protonation-
886 coupled feedback mechanism controls the signalling process in bathy phytochromes. *Nature Chem*
887 **7**:423–430. doi:10.1038/nchem.2225

888 Weissleder R. 2001. A clearer vision for *in vivo* imaging. *Nat Biotech* **19**:316–317. doi:10.1038/86684

889 Xu Q, Vogt A, Frechen F, Yi C, Küçükerden M, Ngum N, Sitjà-Roqueta L, Greiner A, Parri R, Masana M, Wenger
890 N, Wachten D, Möglich A. 2024. Engineering Bacteriophytochrome-coupled Photoactivated Adenylyl
891 Cyclases for Enhanced Optogenetic cAMP Modulation. *J Mol Biol*, Photosensory Receptors-Mechanisms
892 and Effects **436**:168257. doi:10.1016/j.jmb.2023.168257

893 Yang C, Cui M, Zhang Y, Pan H, Liu J, Wang S, Ma N, Chang J, Sun T, Wang H. 2020. Upconversion optogenetic
894 micro-nanosystem optically controls the secretion of light-responsive bacteria for systemic immunity
895 regulation. *Commun Biol* **3**:1–14. doi:10.1038/s42003-020-01287-4

896 Yang X, Kuk J, Moffat K. 2008. Crystal structure of Pseudomonas aeruginosa bacteriophytochrome:
897 Photoconversion and signal transduction. *Proc Natl Acad Sci U S A* **105**:14715–14720.

898 Yi C, Meier SSM, Kehr M, Möglich A. 2025. Spectroscopic Analyses of Photoconversion in Phytochromes. *Meth*
899 *Mol Biol* **submitted**.

900 Ziegler T, Möglich A. 2015. Photoreceptor engineering. *Front Mol Biosci* **2**:30. doi:10.3389/fmolb.2015.00030

901 Zienicke B, Molina I, Glenz R, Singer P, Ehmer D, Escobar FV, Hildebrandt P, Diller R, Lamparter T. 2013. Unusual
902 Spectral Properties of Bacteriophytochrome Agp2 Result from a Deprotonation of the Chromophore in
903 the Red-absorbing Form Pr*. *J Biol Chem* **288**:31738–31751. doi:10.1074/jbc.M113.479535

904 **Acknowledgements**

905 We thank our colleagues for discussion; Dr. Roman S. Iwasaki, Dr. Ralph P. Diensthuber, and Tobias
906 von Basse for preliminary experiments; Tino Krell for generously providing the pMIR66 and pMIR77
907 plasmids; and Mr. Braun and the electronical workshop at University Bayreuth for support. Funding
908 was provided by the European Commission (FET Open NEUROPA grant 863214 to A.M.); the German
909 Research Foundation (grants MO2192/4-2 to A.M. and UE200/1-1 to R.U.); and the Research Council
910 of Finland (grant 330678 to H.T.).

911 **Author Contributions**

912 S.S.M.M. and A.M. conceived of the project; H.T., R.U., and A.M. acquired funding; S.S.M.M., M.H.,
913 C.B., R.U., and A.M. designed research; S.S.M.M., M.H., C.B., E.L.R.D., R.U., and A.M. conducted
914 research; S.S.M.M., M.H., C.B., E.L.R.D., R.U., and A.M. analyzed data; S.S.M.M. and A.M. wrote the
915 manuscript; all authors edited the manuscript.

916 **Competing Interests**

917 The authors declare no competing interests.

Figure Legends

Figure 1

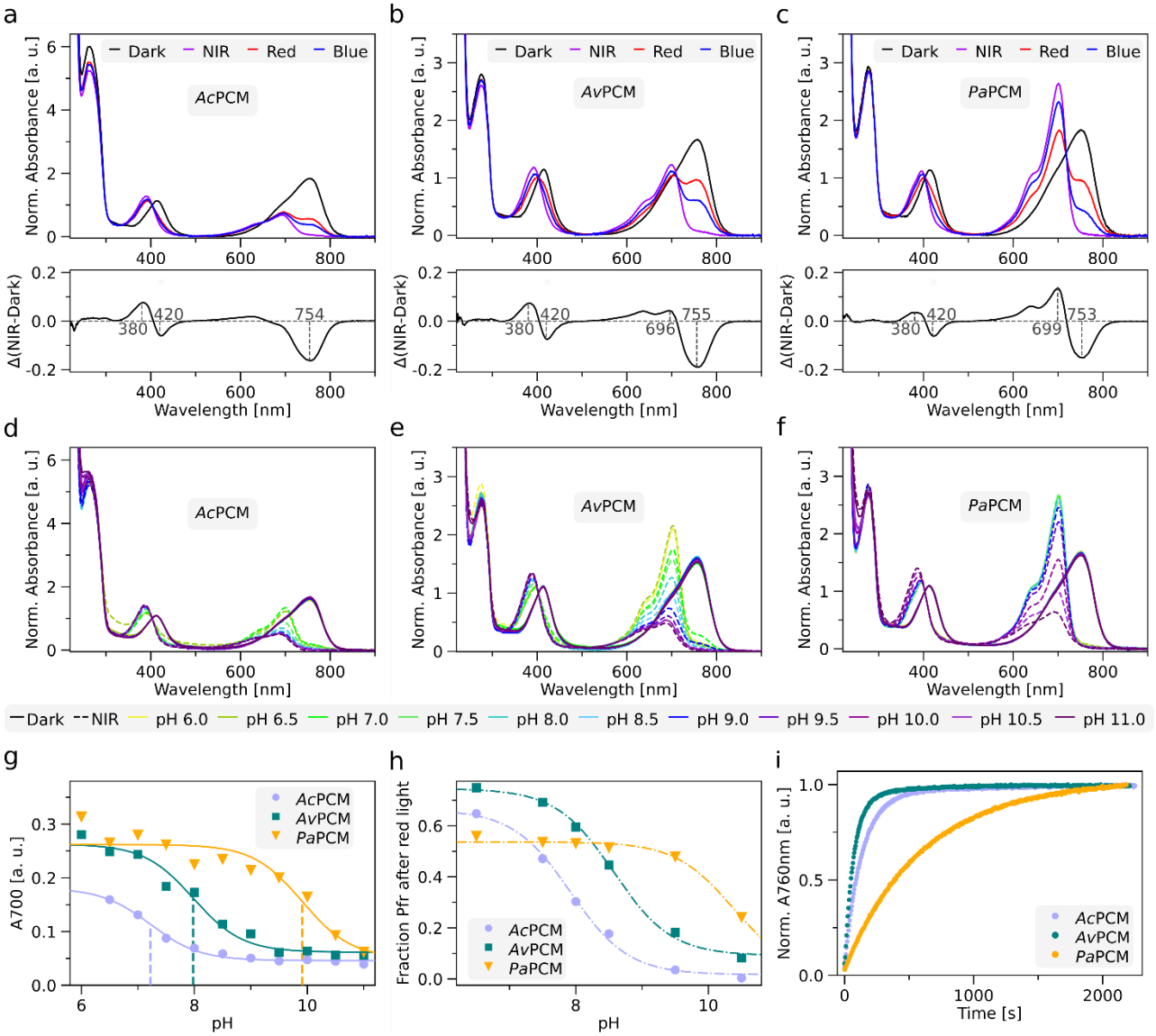

Spectroscopic characterization of bacteriophytochrome photosensory core modules (PCM) from *Azorhizobium caulinodans* (*Ac*PCM), *Agrobacterium vitis* (*Av*PCM), and *Pseudomonas aeruginosa* (*Pa*PCM). (a) UV/vis absorbance spectra of *Ac*PCM at pH 8 in darkness (black line), and after illumination with near-infrared (NIR, purple line), red (red), and blue light (blue). Data are normalized to the absorbance at 403 nm within the Soret band. The lower panel shows the NIR-dark difference absorbance spectrum with maxima and minima marked. (b) and (c) as in (a) but for *Av*PCM and *Pa*PCM. (d) Absorbance spectra of *Ac*PCM in darkness (solid lines) and after NIR illumination (dashed

928 lines) at different pH values as indicated by color. (e) and (f) as in (d) but for *Av*PCM and *Pa*PCM. (g)
929 Absorbance at 700 nm for *Ac*PCM (light purple circles), *Av*PCM (dark green squares), and *Pa*PCM
930 (orange triangles) upon NIR-light exposure at different pH values. Data were fitted to the Henderson-
931 Hasselbalch equation to determine apparent pK_a values (dashed lines, *Ac*PCM: 7.2 ± 0.1, *Av*PCM: 8.0
932 ± 0.1, *Pa*PCM: 9.9 ± 0.2). (h) Calculated Pfr fractions of *Ac*PCM (light purple circles), *Av*PCM (dark
933 green square), and *Pa*PCM (orange triangles) after red-light exposure at different pH values. The
934 underlying absorbance spectra are shown in Suppl. Fig. 1a-c. (i) Dark-recovery kinetics at 25°C and
935 pH 8 after NIR-illumination as followed by absorbance at 760 nm. Time constants for *Ac*PCM (light
936 purple), *Av*PCM (dark green), and *Pa*PCM (orange) were determined by single-exponential fits.

937 **Figure 2**

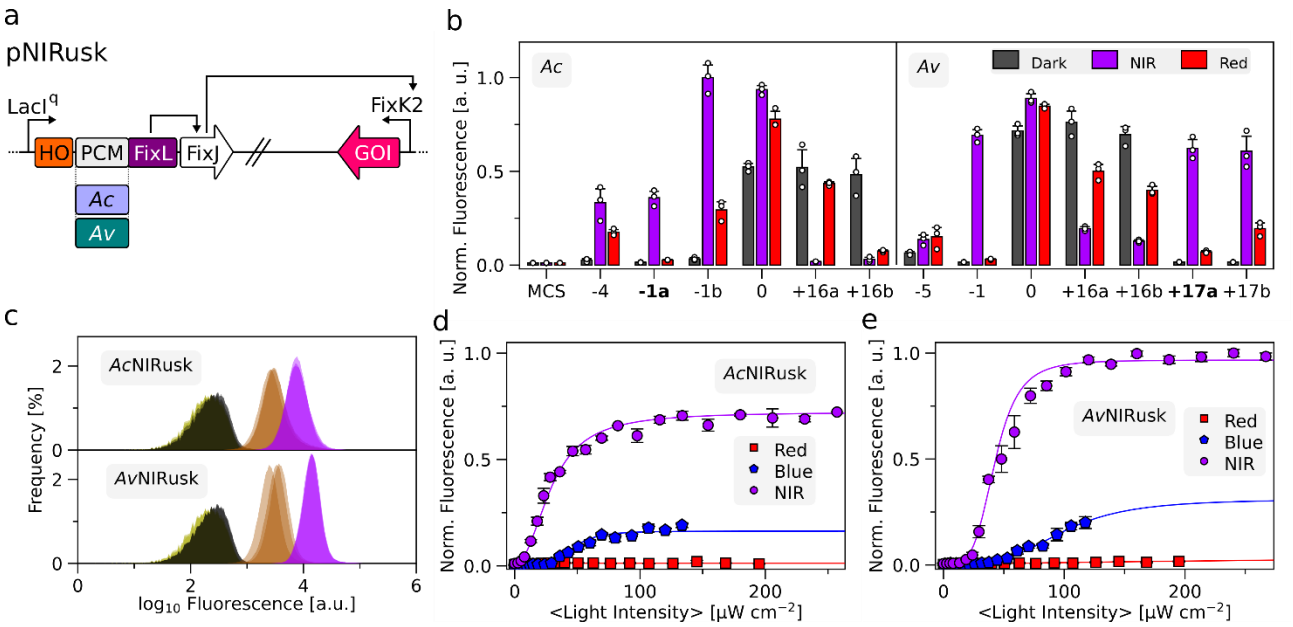

938

939 Engineering of light-regulated sensor histidine kinases (SHK) based on photosensory core modules
940 (PCM) from bathy-bacteriophytochromes (BphP). (a) Schematic of the pNIRusk plasmids to control
941 gene expression in bacteria by NIR light. The LacI^q promoter constitutively expresses a tricistronic
942 operon consisting of heme oxygenase (HO1), the light-regulated SHK (chimera of *Ac*/*Av*PCM and
943 FixL), and the response regulator FixJ. When phosphorylated, FixJ binds to the FixK2 promoter and
944 triggers the expression of a gene of interest (GOI). (b) Response of select *Ac*NIRusk (left) and
945 *Av*NIRusk (right) systems to different light conditions (grey: darkness; purple: NIR light; red: red
946 light). *Ds*Red reporter fluorescence was normalized to the optical density of the bacterial cultures.
947 Individual pNIRusk variants are denoted by the relative lengths of the linkers within their underlying
948 SHKs (see Suppl. Fig. 3), with the variants chosen for further analyses highlighted in bold. As control,
949 an empty-vector construct (MCS) is shown, and data are normalized to the maximal fluorescence.
950 (c) Flow-cytometric analyses of bacteria containing *Ac*NIRusk-1a (top) or *Av*NIRusk+17a (bottom)
951 upon incubation in darkness (black), moderate NIR (brown), or strong NIR light (purple) (also see
952 Suppl. Fig. 5). An empty-vector control (MCS) is shown in green. (d) Light-dose response of bacteria

containing *Ac*NIRusk-1a incubated in NIR (purple circles), red (red squares), and blue light (blue pentagons). (e) as in (d) but for *Av*NIRusk+17a.

955 **Figure 3**

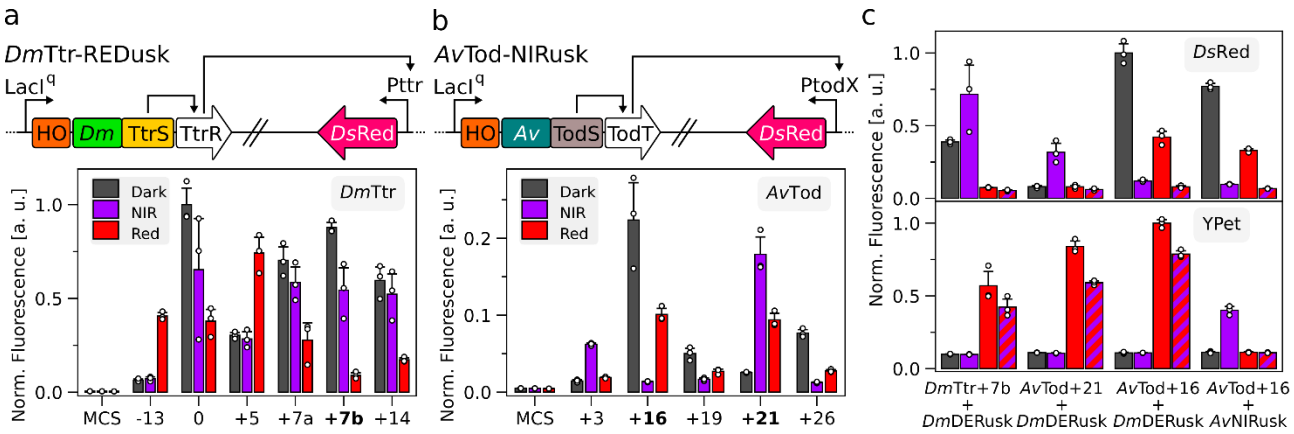

956

957 Engineering of orthogonal light-regulated two-component systems (TCS). (a) Schematic of the
958 *Dm*Ttr-REDusk circuit based on the TtrSR TCS from *Shewanella baltica* combined with the
959 photosensory core module (PCM) from the *Deinococcus maricopensis* bacteriophytochrome (BphP)
960 (top). Reporter fluorescence of bacteria bearing circuits with different linker lengths of their
961 underlying sensor histidine kinases (SHK) upon cultivation in darkness (grey), NIR (purple), and red
962 light (red) (bottom). An empty-vector control is denoted as 'MCS', and data are normalized to the
963 maximal fluorescence. Variants are marked by the relative lengths of the linkers within their
964 underlying SHKs compared to pREDusk (see Suppl. Fig. 6). Variants characterized further are
965 highlighted in bold. (b) as in (a) but for the *Av*Tod-NIRusk circuit based on the TodST TCS from
966 *Pseudomonas putida* combined with the BphP PCM from *Agrobacterium vitis*. (c) Multiplexing of
967 bacteria containing two optogenetic circuits, as noted below the graph, to separately control the
968 expression of *Ds*Red (top) and YPet (bottom) reporters. After incubation in darkness (gray), NIR
969 (purple), red (red), and combined NIR and red light (red and purple stripes), fluorescence was
970 measured and normalized to the maximal value.

971 **Figure 4**

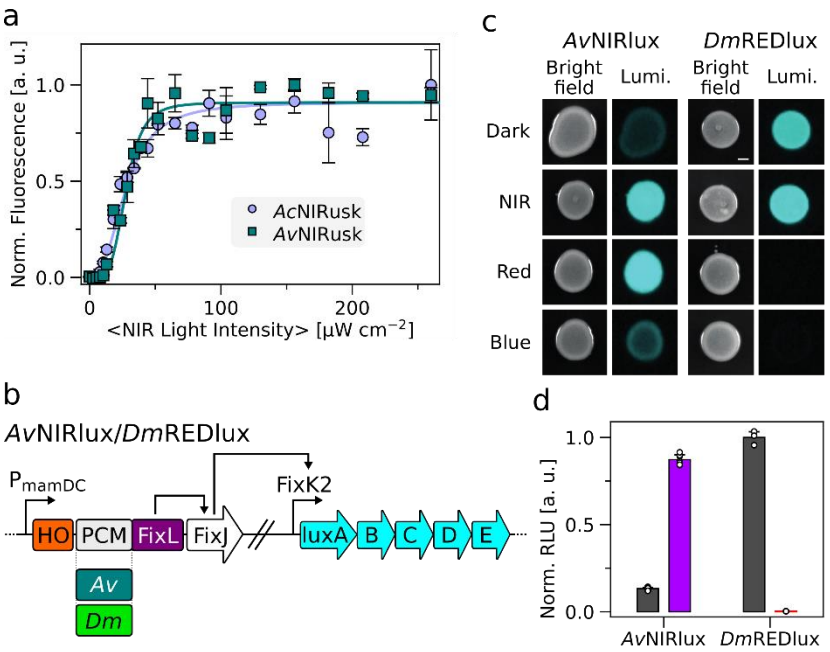

972

973 Light-regulated gene expression in *Escherichia coli* Nissle (*Ec*N) and *Agrobacterium tumefaciens*. (a)
974 Light-dose response of *Ec*N harboring *Ac*NIRusk (light purple circles) and *Av*NIRusk (dark green
975 squares) after incubation at varying NIR-light intensities. (b) Schematic of the *Av*NIRlux and
976 *Dm*REDlux circuits based on *Av*PCM and *Dm*PCM. The tricistronic cassette comprising heme
977 oxygenase (HO1), the sensor histidine kinase (chimera of *Av*/*Dm*PCM and FixL), and FixJ is controlled
978 by the constitutive PmamDC promoter from *Magnetospirillum gryphiswaldense*, whereas the FixK2
979 promoter regulates the expression of the *luxABCDE* operon. (c) *A. tumefaciens* bacteria bearing
980 *Av*NIRlux (left) and *Dm*REDlux (right) were spotted on plates and incubated at different light
981 conditions (darkness, NIR, red, or blue light), followed by luminescence (Lumi.) measurements (see
982 Suppl. Fig. 8a). (d) *A. tumefaciens* bacteria carrying *Av*NIRlux and *Dm*REDlux were incubated in liquid
983 culture for 20 h under different light conditions (gray: darkness, purple: NIR light, red: red light),
984 followed by recording of reporter luminescence (see Suppl. Fig. 8c-d).

985 **Figure 5**

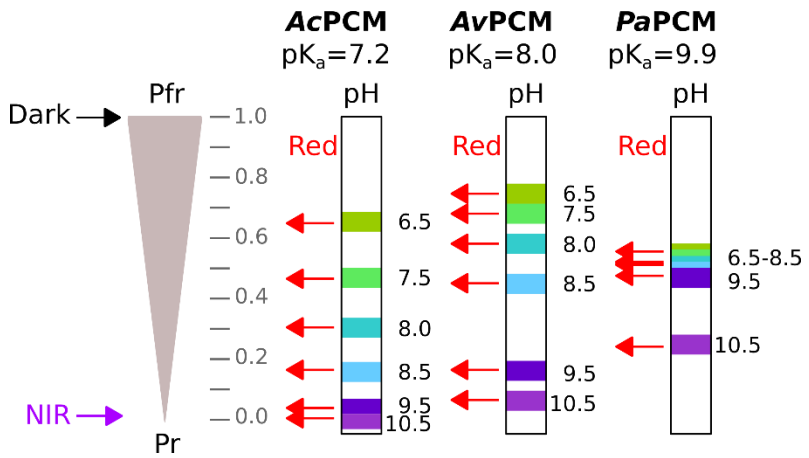

986

987 Photoreception by select bathy-bacteriophytochromes (BphP) at different pH values. Throughout
988 the entire tested pH range, the photosensory core modules (PCM) of the bathy-BphPs from
989 *Azorhizobium caulinodans* (*Ac*PCM), *Agrobacterium vitis* (*Av*PCM), and *Pseudomonas aeruginosa*
990 (*Pa*PCM) adopt a pure Pfr state in darkness with fully protonated biliverdin (BV) chromophore. NIR
991 light drives the complete conversion to the Pr state in which BV can be either protonated or
992 deprotonated as governed by pH and the respective pK_a value of the bathy-BphP. Red light populates
993 a photostationary mixture with Pr and Pfr proportions strongly depending on pH. At high pH values,
994 red light can drive the bathy-BphP nearly completely to the Pr state for *Ac*PCM and *Av*PCM. Owing
995 to a higher pK_a value for BV protonation, *Pa*PCM is less affected but follows the same trend.

Engineering NIR-Sighted Bacteria

Stefanie S. M. Meier[1,‡], Michael Hörzing[1,‡], Cornelia Böhm[2,3,‡], Emma L. R. Düthorn[1,‡], Heikki Takala[2,‡], René Uebe[4,5,‡], Andreas Möglich[1,5,6,*,‡]

[1] Department of Biochemistry, University of Bayreuth, 95447 Bayreuth, Germany.
[2] Department of Biological and Environmental Science, Nanoscience Center, University of Jyvaskyla, Jyvaskyla 40014, Finland.
[3] Institute of Biochemistry, Graz University of Technology, 8010 Graz, Austria
[4] Department of Microbiology, University of Bayreuth, 95447 Bayreuth, Germany.
[5] Bayreuth Center for Biochemistry & Molecular Biology, Universität Bayreuth, 95447 Bayreuth, Germany.
[6] North-Bavarian NMR Center, Universität Bayreuth, 95447 Bayreuth, Germany.

* for correspondence: andreas.moeglich@uni-bayreuth.de
‡ ORCID identifiers: S.S.M.M. 0009-0002-6028-5223; M.H. 0009-0008-2301-3783; C.B. 0000-0002-3552-2349; E.L.R.D. 0009-0000-4156-5428; H.T. 0000-0003-2518-8583; R.U. 0000-0003-2357-1589; A.M. 0000-0002-7382-2772

Table of Contents

Supplementary Figure 1 _____ 3

Supplementary Figure 2 _____ 5

Supplementary Figure 3 _____ 6

Supplementary Figure 4 _____ 7

Supplementary Figure 5 _____ 8

Supplementary Figure 6 _____ 9

Supplementary Figure 7 _____ 10

Supplementary Figure 8 _____ 12

Supplementary Figure 9 _____ 13

Supplementary Table 1 _____ 14

Supplementary Table 2 _____ 21

Supplementary References _____ 23

Supplementary Figure 1

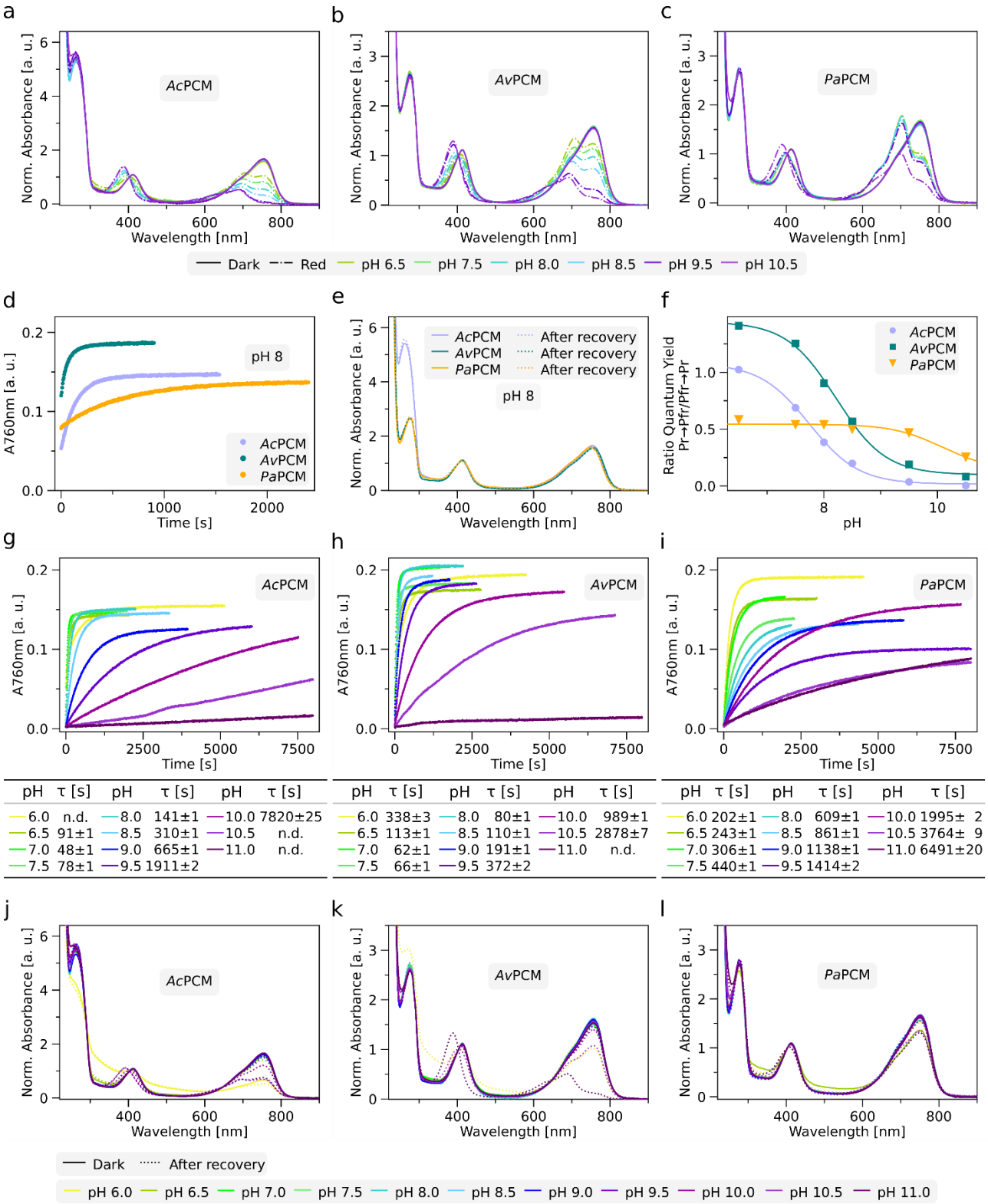

pH	τ [s]	pH	τ [s]	pH	τ [s]
6.0	n.d.	8.0	141±1	10.0	7820±25
6.5	91±1	8.5	310±1	10.5	n.d.
7.0	48±1	9.0	665±1	11.0	n.d.
7.5	78±1	9.5	1911±2		

pH	τ [s]	pH	τ [s]	pH	τ [s]
6.0	338±3	8.0	80±1	10.0	989±1
6.5	113±1	8.5	110±1	10.5	2878±7
7.0	62±1	9.0	191±1	11.0	n.d.
7.5	66±1	9.5	372±2		

pH	τ [s]	pH	τ [s]	pH	τ [s]
6.0	202±1	8.0	609±1	10.0	1995± 2
6.5	243±1	8.5	861±1	10.5	3764± 9
7.0	306±1	9.0	1138±1	11.0	6491±20
7.5	440±1	9.5	1414±2		

Additional spectroscopic characterization of bacteriophytochrome photosensory core modules (PCM) from *Azorhizobium caulinodans* (*Ac*PCM), *Agrobacterium vitis* (*Av*PCM), and *Pseudomonas aeruginosa* (*Pa*PCM). (a) Absorbance spectra of *Ac*PCM at different pH values as indicated below the

graph in darkness (solid line) and after red-light-illumination (dotted line). Data are normalized to the absorbance at 403 nm within the Soret band. (b) and (c) as in (a) but for *Av*PCM and *Pa*PCM. (d) Dark-recovery kinetics of *Ac*PCM (light purple circles), *Av*PCM (dark green circles), and *Pa*PCM (orange circles) monitored at 760 nm, 25°C, and pH 8 after illumination with red light. Time constants determined by single-exponential fits are (147 ± 1) s, (71 ± 1) s and (599 ± 2) s for *Ac*PCM, *Av*PCM, and *Pa*PCM, respectively. (e) Absorbance spectra recorded in darkness (solid lines) and after dark recovery (dotted lines) for *Ac*PCM (light purple), *Av*PCM (dark green), and *Pa*PCM (orange) at pH 8. (f) Ratio of the quantum yields for Pr→Pfr over Pfr→Pr photoconversion as a function of pH. (g) Dark-recovery kinetics of *Ac*PCM recorded at 760 nm after illuminating with NIR light at 25°C and different pH as indicated below the graph. Time constants were determined by single-exponential fits, with the results shown in the table. (h) and (i) as in (g) but for *Av*PCM and *Pa*PCM. (j) Absorbance spectra of *Ac*PCM recorded in darkness (solid lines) and after dark recovery (dotted lines) at different pH as indicated below the graph. (k) and (l) as in (j) but for *Av*PCM and *Pa*PCM.

Supplementary Figure 2

```
                                PCM                                  Linker FixL
                                                                    |
DmREDusk   TPRASFSSYVEAVRGVAQPWQAGDLDAALDLRGALLEVQGARLLQELQSELVHVSRLSAM  527
AcNIRusk-0 TPRKSFAIWKETVEHQSWPWTQADRDFAEAARNALVEIVLRHNLQELQSELVHVSRLSAM  518
AvNIRusk-0 TPRKSFAIWKEAVTKQSDHWSENDREVAEAIRAVTVKVVLRHNLQELQSELVHVSRLSAM  516
           *** **: : *:*   :  *   * : *   * . :::   : *****************
                  ▼
DmREDusk   GEMASALAHELNQPLAAISNYMKGSRRLLAGSSDPNTPKVESALDRAAEQALRAGQIIRR  587
AcNIRusk-0 GEMASALAHELNQPLAAISNYMKGSRRLLAGSSDPNTPKVESALDRAAEQALRAGQIIRR  578
AvNIRusk-0 GEMASALAHELNQPLAAISNYMKGSRRLLAGSSDPNTPKVESALDRAAEQALRAGQIIRR  576
           ************************************************************
                    |
                    FixL
```

Multiple sequence alignment of the sensor histidine kinases within *Dm*REDusk, *Ac*NIRusk+0, and *Av*NIRusk+0. The different shading marks the fusion of the photosensory core modules (PCM) of the bacteriophytochromes from *Deinococcus maricopensis* (*Dm*PCM), *Azorhizobium caulinodans* (*Ac*PCM), and *Agrobacterium vitis* (*Av*PCM) with the catalytic domains of the sensor histidine kinase FixL from *Bradyrhizobium japonicum*. The linker region is shown in pink, and the active-site histidine is marked with a red triangle.

Supplementary Figure 3

a

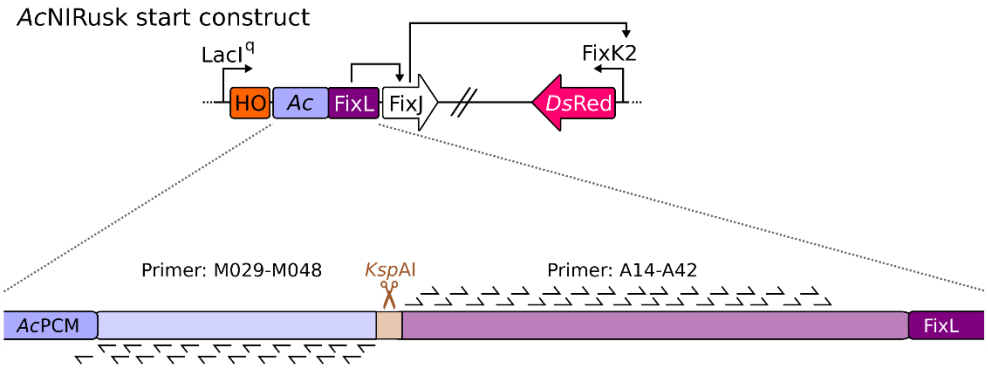

Plasmid	Label	501	257	291	Expression
MH013	sc	VLRHN ELLADERGKADVRQRLLNE	TEHQQTQARLQELQSELVHVSRLSAMGEMASALA	HELN	No
MH021	−4	VLRHN ELLADERG	RLSAMGEMASALA	HELN	NIR/Red
MH019	−1a	VLRHN ELLAD	ELVHVSRLSAMGEMASALA	HELN	NIR
MH034	−1b	VLRHN ELL	QSELVHVSRLSAMGEMASALA	HELN	NIR/Red
MH005	0	VLRHN	LQELQSELVHVSRLSAMGEMASALA	HELN	Dark/NIR/Red
MH017	+16a	VLRHN ELLADER	TEHQQTQARLQELQSELVHVSRLSAMGEMASALA	HELN	Dark/Red
MH018	+16b	VLRHN ELLADERG	EHQQTQARLQELQSELVHVSRLSAMGEMASALA	HELN	Dark

b

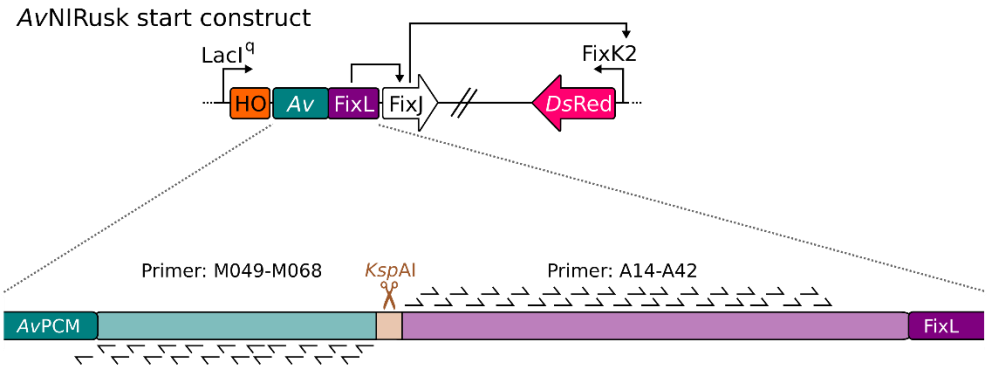

Plasmid	Label	499	257	291	Expression
MH014	sc	VLRHN ELMQEERNKADIRQRVLNE	TEHQQTQARLQELQSELVHVSRLSAMGEMASALA	HELN	No
MH030	−5	VLRHN ELMQEER	RLSAMGEMASALA	HELN	NIR/Red
MH023	−1	VLRHN ELMQE	ELVHVSRLSAMGEMASALA	HELN	NIR
MH006	0	VLRHN	LQELQSELVHVSRLSAMGEMASALA	HELN	Dark/NIR/Red
MH029	+16a	VLRHN ELMQEERN	EHQQTQARLQELQSELVHVSRLSAMGEMASALA	HELN	Dark/Red
MH020	+16b	VLRHN ELMQEER	TEHQQTQARLQELQSELVHVSRLSAMGEMASALA	HELN	Dark/Red
MH028	+17a	VLRHN ELMQEER<u>K</u>	TEHQQTQARLQELQSELVHVSRLSAMGEMASALA	HELN	NIR
MH038	+17b	VLRHN ELMQEERN	TEHQQTQARLQELQSELVHVSRLSAMGEMASALA	HELN	NIR/Red

*Ac*NIRusk (a) and *Av*NIRusk (b) PATCHY start constructs (sc) and derived linker variants. The linker between the *Ac*/*Av*PCM and FixL was adopted from the parental proteins and is defined as the region between the PCM (residues VLRHN) and the active-site histidine at position 291. At the junction, a *Ksp*AI restriction site and a frameshift were inserted. Underlined amino acids originate from a cloning artifact. PATCHY primers are listed in Suppl. Table 1.

Supplementary Figure 4

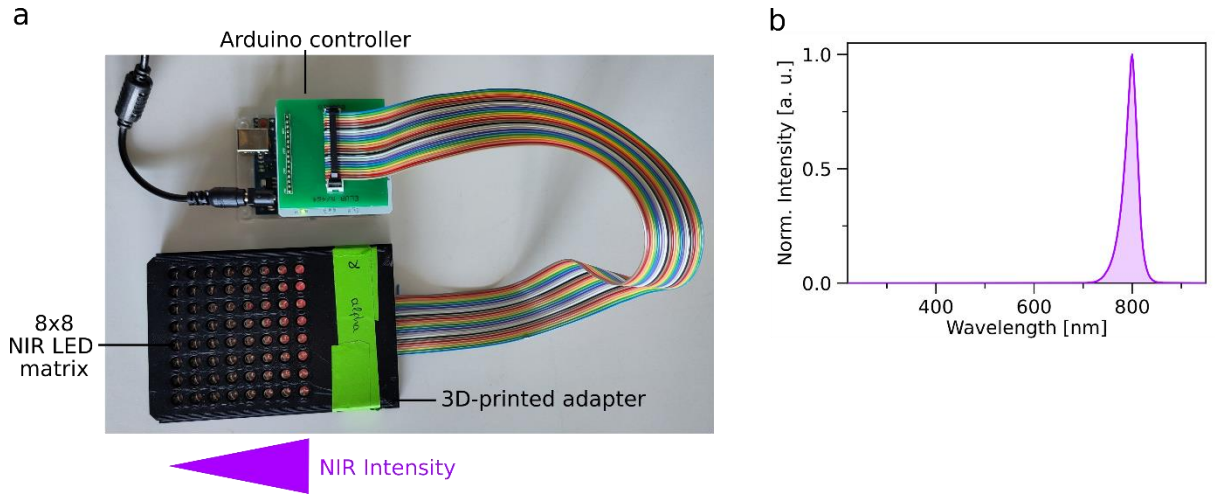

Setup for illumination with near-infrared (NIR) light at different intensities in a microtiter-plate (MTP) format. (a) The programmable 8-by-8 matrix of NIR light-emitting diodes (LED) is based on a previous setup (Hennemann et al., 2018; Stüven et al., 2019) and integrated into a 3D-printed adapter. NIR-light intensities can be adjusted by an Arduino microcontroller. (b) Emission spectrum of the NIR LED matrix with a maximum at 800 nm and a full width at half-maximum of 18 nm.

Supplementary Figure 5

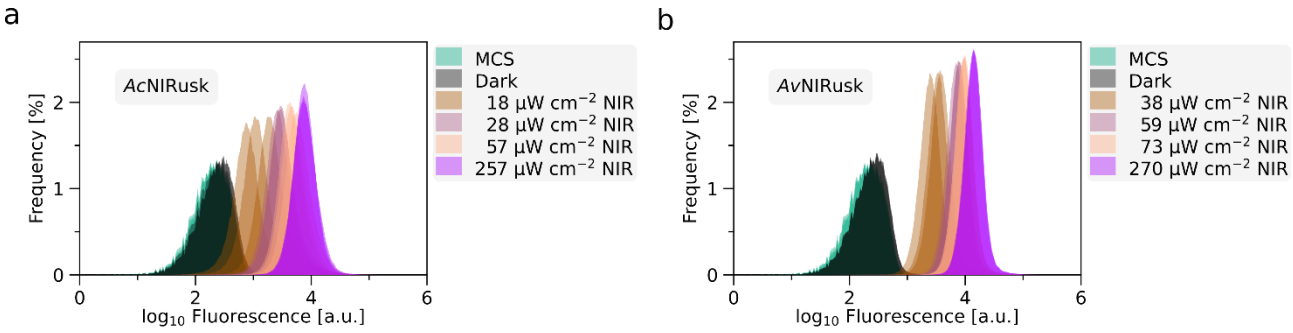

Analyses by flow cytometry of *Ds*Red production of bacteria containing *Ac*NIRusk (a) or *Av*NIRusk (b) when incubated in darkness (black), or under different NIR-light intensities. An empty-vector control (MCS) is shown in green.

Supplementary Figure 6

a

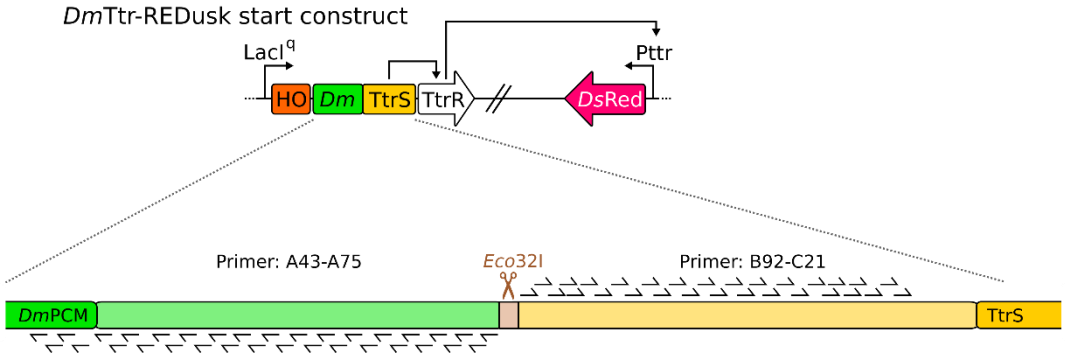

Plasmid	Label	510 … 407 … 441	Expression
SM123	sc	GARL AALQDLNARLERANRELEGRNAELRRFAF RELINTQRQLNENRALLEHAQRIAIAGELGASLS HELN	No
SM146	−13	GARL A AIAGELGASLS HELN	Red
SM147	0	GARL LNENRALLEHAQRIAIAGELGASLS HELN	Dark/NIR
SM148	+5	GARL AA QRQLNENRALLEHAQRIAIAGELGASLS HELN	Red
SM149	+7a	GARL A INTQRQLNENRALLEHAQRIAIAGELGASLS HELN	Dark/NIR
SM150	+7b	GARL AALQDLNARLERANRELEGRNAELRR LGASLS HELN	Dark/NIR
SM153	+14	GARL AALQDLNARLERANRELEGRNAELRRFAFD AGELGASLS HELN	Dark/NIR

b

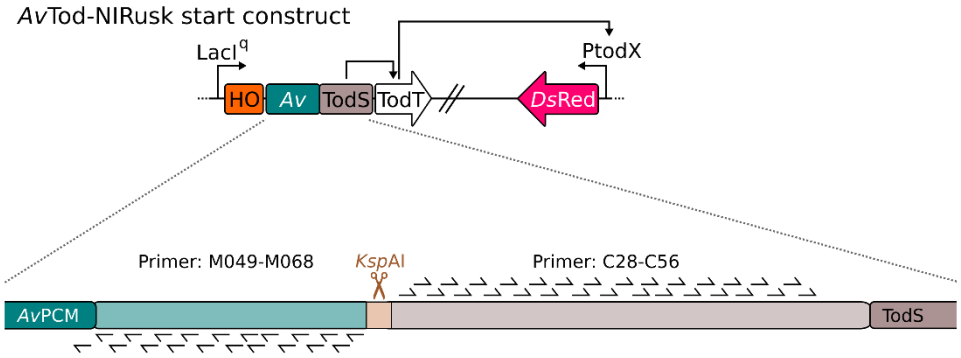

Plasmid	Label	499 … 726 … 760	Expression
SM128	sc	VLRHN ELMQEERNKADIRQRVLNE TEKKQAQENLNQLQQQLVYVSRSATMGEFAAYIA HEIN	No
SM160	+3	VLRHN ELMQEERNKADIRQRVLNE MGEFAAYIA HEIN	NIR
SM161	+16	VLRHN ELMQEERNKADIRQRVLNEV QQQLVYVSRSATMGEFAAYIA HEIN	Dark/Red
SM162	+19	VLRHN ELMQEERNKADIRQRVLNEV NQLQQQLVYVSRSATMGEFAAYIA HEIN	Dark
SM163	+21	VLRHN ELMQEERNKADIRQR KQAQENLNQLQQQLVYVSRSATMGEFAAYIA HEIN	NIR/Red
SM164	+26	VLRHN ELMQEERNKADIRQRVL TEKKQAQENLNQLQQQLVYVSRSATMGEFAAYIA HEIN	Dark/Red

*Dm*Ttr-REDusk (a) and *Av*Tod-NIRusk (b) PATCHY start constructs (sc) and derived linker variants. The linker between the *Dm*/*Av*PCM and the TtrS/TodS two-component system was adopted from the natural proteins. At the junction, a *Eco*32I or *Ksp*AI restriction site and a frameshift were inserted. Underlined amino acids highlighted derive from a cloning artifact. PATCHY primers are listed in Suppl. Table 1.

Supplementary Figure 7

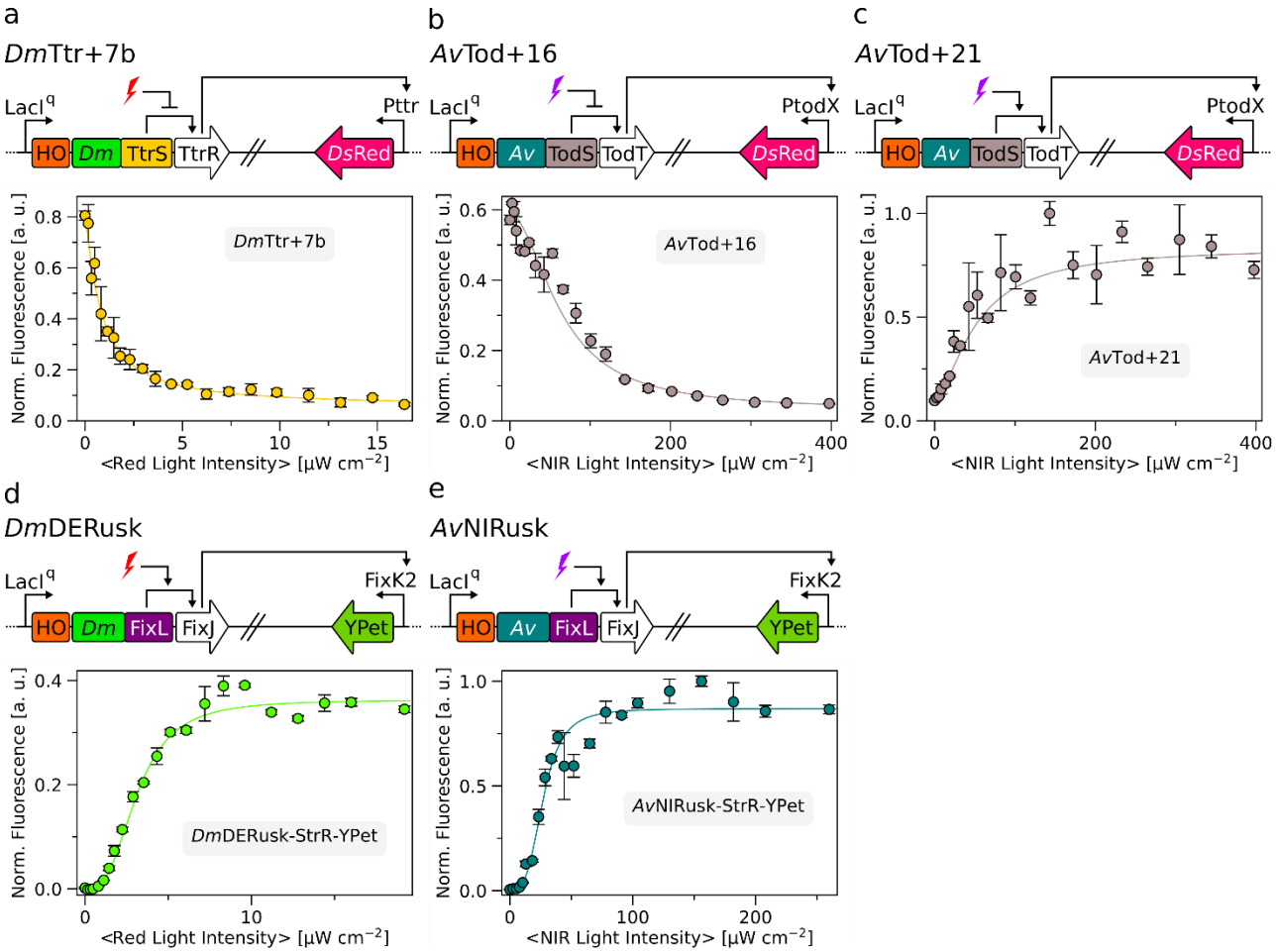

f

	Dark	NIR	Red	NIR+Red
*Dm*Ttr+7b-*Ds*Red + *Dm*DERusk-YPet	*Ds*Red	*Ds*Red	YPet	YPet
*Av*Tod+21-*Ds*Red + *Dm*DERusk-YPet		*Ds*Red	YPet	YPet
*Av*Tod+16-*Ds*Red + *Dm*DERusk-YPet	*Ds*Red		*Ds*Red, YPet	YPet
*Av*Tod+16-*Ds*Red + *Av*NIRusk-YPet	*Ds*Red	YPet	*Ds*Red	

Characterization of constructs used in multiplexing experiments. (a) Schematic of *Dm*Ttr+7b (top) and associated light-dose response (bottom). (b) and (c) as in (a) but for *Av*Tod+16 and *Av*Tod+21. Data in panels a-c are normalized to the maximal fluorescence obtained for *Av*Tod+21. (d) Schematic of *Dm*DERusk-StrR-YPet (top) and the associated light-dose response (bottom). (e) as in (d) but for *Av*NIRusk-StrR-YPet. Data in panels d-f are normalized to the maximal fluorescence obtained for of *Av*NIRusk-StrR-YPet. (f) The schematic summarizes the results of the multiplexing experiments from

Fig. 3c. The production of *Ds*Red and YPet under different light conditions are shown by pink pentagons and green heptagons, respectively.

Supplementary Figure 8

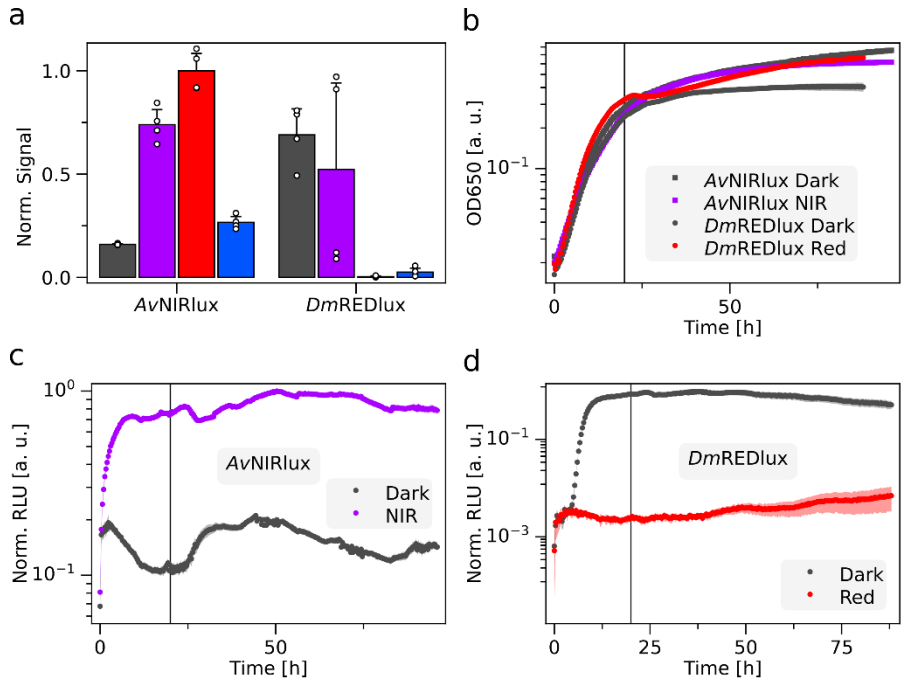

Gene expression regulated by *Av*NIRlux and *Dm*REDlux in *Agrobacterium tumefaciens*. (a) Quantified luminescence from the spotting assay in Fig. 4b. Bar colors represent incubation in darkness (gray), NIR (purple), red (red), or blue (blue) light. (b) Optical density at 650 nm of *A. tumefaciens* bacteria bearing *Av*NIRlux or *Dm*REDlux grown in liquid culture under different light conditions. (c) Normalized reporter luminescence of the bacteria from panel (b) harboring *Av*NIRlux and grown in darkness (grey) or under NIR light (purple). The vertical black line denotes a time point of 20 h on which the data in Fig. 4d are based. (d) as for (c) but for *A. tumefaciens* bacteria containing *Dm*REDlux and illumination with red instead of NIR light (red).

Supplementary Figure 9

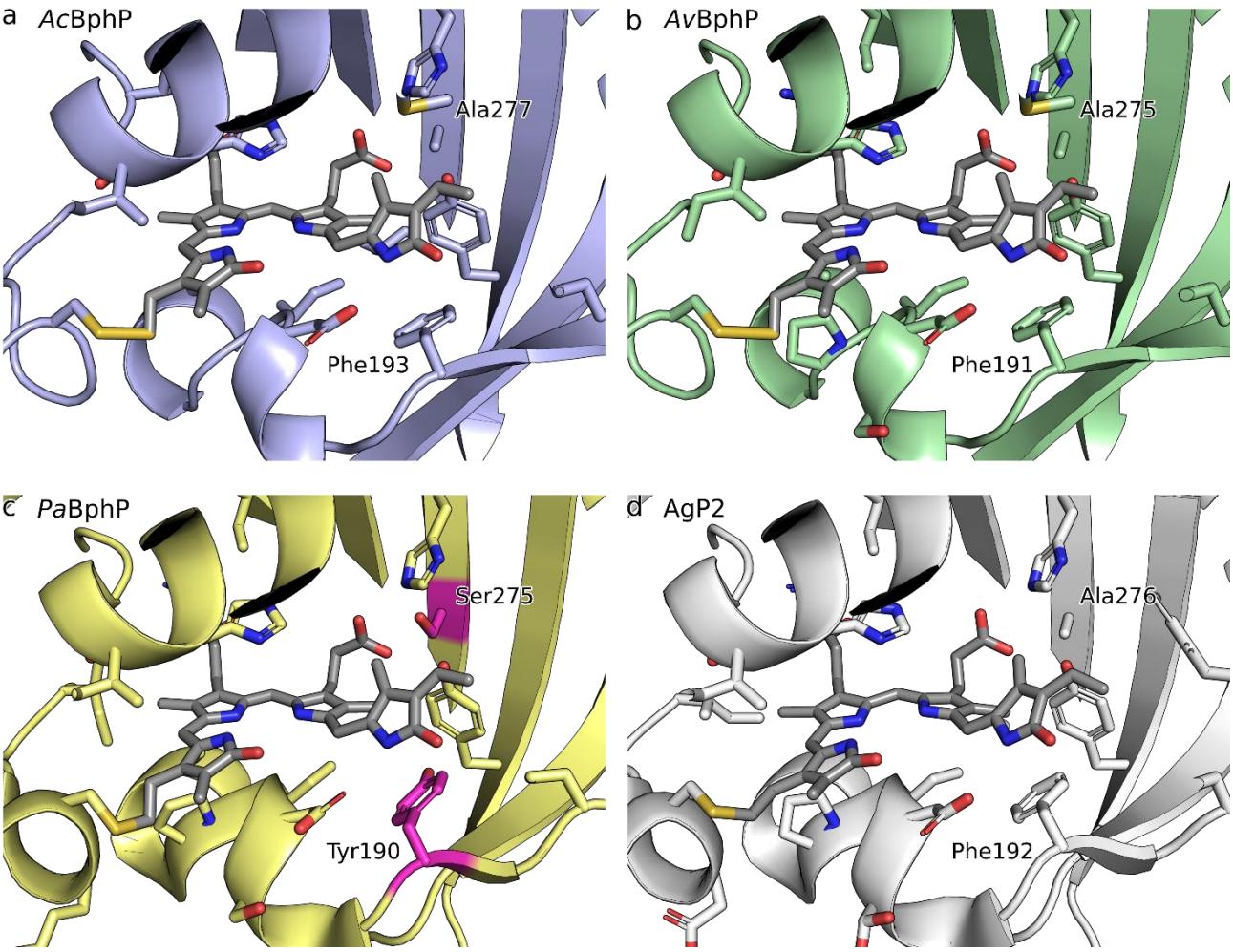

Biliverdin binding pocket in the photosensory core modules (PCM) of (a) *Azorhizobium caulinodans* bacteriophytochrome (BphP), (b) *Agrobacterium vitis* BphP, (c) *Pseudomonas aerugionsa* BphP, and (d) *Agrobacterium tumefaciens* Agp2 BphP. Whereas experimental structures are available for the PCMs of AgP2 [PDB entry 6g1y (Schmidt et al., 2018)] and *Pa*BphP [3c2w (Yang et al., 2008)], for *Ac*BphP and *Av*BphP, PCM models were calculated with AlphaFold3 (Abramson et al., 2024). Tyrosine 190 and serine 275 are highlighted in the *Pa*PCM structure by magenta color. The other three PCMs feature less polar phenylalanine and alanine residues, respectively, in the structurally equivalent positions.

Supplementary Table 1

Oligonucleotides used in this study. Overhang regions are indicated in bold, and restriction enzyme recognition sites are underlined.

Name	**Sequence 5'-3'**
Primers for cloning of bathy-PCM expression constructs	
M001_Ac_Bb_for	CCTGGTTGAAATTGTGCTGCGTCATAATGAGAATCTTTATTTTCAGCATCACCA
M002_Ac_Bb_rev	GATCAACTGCTTCTGCATTCGGCATGGTATATCTCCTTATTAAAGTTAAACAAAA
M003_Ac_Ins_for	TTTTGTTTAACTTTAATAAGGAGATATACCATGCCGAATGCAGAAGCAGTTGATC
M004_Ac_Ins_rev	TGGTGATGCTGAAAATAAAGATTCTCATTATGACGCAGCACAATTTCAACCAGG
M005_Av_Bb_for	ACCGTTAAAGTGGTTCTGCGCCATAATGAGAATCTTTATTTTCAGCATCACCA
M006_Av_Bb_rev	ATCAACGGTCTGGGTTGCAGGCATGGTATATCTCCTTATTAAAGTTAAACAAAA
M007_Av_Ins_for	TTTTGTTTAACTTTAATAAGGAGATATACCATGCCTGCAACCCAGACCGTTGAT
M008_Av_Ins_rev	TGGTGATGCTGAAAATAAAGATTCTCATTATGGCGCAGAACCACTTTAACGGT
M069_Pa-Ins-fw	TTTTGTTTAACTTTAATAAGGAGATATACCATGACGAGCATCACCCCGGTTACCC
M070_Pa-Ins-rev	TGGTGATGGCCCTGAAAATAAAGATTCTCCGCATGGTTGAGGCACAGTTCCATC
M071_Pa-Bb-fw	GATGGAACTGTGCCTCAACCATGCGGAGAATCTTTATTTTCAGGGCCATCACCA
M072_Pa-Bb-rev	GGGTAACCGGGGTGATGCTCGTCATGGTATATCTCCTTATTAAAGTTAAACAAAA
M017_AcAv_TEVrepair_fw	GGCCATCACCATCACCATCACCATCAC
M018_Ac_TEVrepair_rev	CTGAAAATAAAGATTCTCATTATGACGC
M019_Av_TEVrepair_rev	CTGAAAATAAAGATTCTCATTATGGCGC
Primers for Gibson cloning of bathy-PCMs into pREDusk	
M009_Ac_Bb_for	CCTGGTTGAAATTGTGCTGCGTCATAATCTCCAGGAACTGCAATCCGAGCTCGTC
M010_Ac_Bb_rev	TTGTCAGATCAACTGCTTCTGCATTCGTCATGCGTGGGCGACCTCAGGC
M011_Ac_Ins_for	GCCTGAGGTCGCCCACGCATGACGAATGCAGAAGCAGTTGATCTGACAA
M012_Ac_Ins_rev	GACGAGCTCGGATTGCAGTTCCTGGAGATTATGACGCAGCACAATTTCAACCAGG

Name	**Sequence 5'-3'**
M013_Av_Bb_for	CCGTTAAAGTGGTTCTGCGCCATAATCTCCAGGAACTGCAATCCGAGCTCGTC
M014_Av_Bb_rev	GTCAGATCAACGGTCTGGGTTGCAGTCATGCGTGGGCGACCTCAGGC
M015_Av_Ins_for	GCCTGAGGTCGCCCACGCATGACTGCAACCCAGACCGTTGATCTGAC
M016_Av_Ins_rev	GACGAGCTCGGATTGCAGTTCCTGGAGATTATGGCGCAGAACCACTTTAACGG
Primers for cloning of PATCHY *Ac*/*Av*NIRusk start constructs	
A07_P_I_II_Step1_for	TTAACCGAGCATCAGCAGACACAAGCACGTCTCCAGGAACTGCAATCCGAGCTCG
M020_AcREDusk_PATCHY_rev1	CGCTCGTCAGCCAGTAATTCATTATGACGCAGCACAATTTCAACC
M021_AcREDusk_PATCHY_rev2	GACGCACGTCTGCTTTCCCGCGCTCGTCAGCCAGTAATTCATTAT
M022_AcREDusk_PATCHY_fw2	AGCGTCTTCTTAATGAAGTTAACCGAGCATCAGCAGACACAAG
M023_AvREDusk_PATCHY_rev1	CGCTCCTCTTGCATCAGTTCATTATGGCGCAGAACCACTTTAACG
M025_AvREDusk_PATCHY_fw2	AGCGTGTCTTAAACGAGGTTAACCGAGCATCAGCAGACACAAG
M028_AvREDusk_PATCHY_rev2	GACGAATGTCTGCTTTGTTACGCTCCTCTTGCATCAGTTCATTAT
PATCHY forward primers for amplification of FixL	
A14_P_I_II_for_1	ACCGAGCATCAGCAGAC
A15_P_I_II_for_2	GAGCATCAGCAGACACAAG
A16_P_I_II_for_3	CATCAGCAGACACAAGC
A17_P_I_II_for_4	CAGCAGACACAAGCACG
A18_P_I_II_for_5	CAGACACAAGCACGTCTC
A19_P_I_II_for_6	ACACAAGCACGTCTCC
A20_P_I_II_for_7	CAAGCACGTCTCCAGG
A21_P_I_II_for_8	GCACGTCTCCAGGAAC
A22_P_I_II_for_9	CGTCTCCAGGAACTGC
A23_P_I_II_for_10	CTCCAGGAACTGCAATCC
A24_P_I_II_for_11	CAGGAACTGCAATCCG
A25_P_I_II_for_12	GAACTGCAATCCGAGC
A26_P_I_II_for_13	CTGCAATCCGAGCTCG
A27_P_I_II_for_14	CAATCCGAGCTCGTCC
A28_P_I_II_for_15	TCCGAGCTCGTCCACG
A29_P_I_II_for_16	GAGCTCGTCCACGTCTC

Name	Sequence 5'-3'
A30_P_I_II_for_17	CTCGTCCACGTCTCCAG
A31_P_I_II_for_18	GTCCACGTCTCCAGGC
A32_P_I_II_for_19	CACGTCTCCAGGCTGAG
A33_P_I_II_for_20	GTCTCCAGGCTGAGCG
A34_P_I_II_for_21	TCCAGGCTGAGCGCCATG
A35_P_I_II_for_22	AGGCTGAGCGCCATGG
A36_P_I_II_for_23	CTGAGCGCCATGGGCG
A37_P_I_II_for_24	AGCGCCATGGGCGAAATG
A38_P_I_II_for_25	GCCATGGGCGAAATGG
A39_P_I_II_for_26	ATGGGCGAAATGGCGTC
A40_P_I_II_for_27	GGCGAAATGGCGTCCG
A41_P_I_II_for_28	GAAATGGCGTCCGCGC
A42_P_I_II_for_29	ATGGCGTCCGCGCTCG
PATCHY forward primers for amplification of TtrS	
B92_P_Ttr_for_01	CGCGAACTGATTAATACCC
B93_P_Ttr_for_02	GAACTGATTAATACCCAGCG
B94_P_Ttr_for_03	CTGATTAATACCCAGCGTCAG
B95_P_Ttr_for_04	ATTAATACCCAGCGTCAGC
B96_P_Ttr_for_05	AATACCCAGCGTCAGC
B97_P_Ttr_for_06	ACCCAGCGTCAGCTGAATG
B98_P_Ttr_for_07	CAGCGTCAGCTGAATG
B99_P_Ttr_for_08	CGTCAGCTGAATGAAAATCG
C01_P_Ttr_for_09	CAGCTGAATGAAAATCGTG
C02_P_Ttr_for_10	CTGAATGAAAATCGTGCACTG
C03_P_Ttr_for_11	AATGAAAATCGTGCACTGC
C04_P_Ttr_for_12	GAAAATCGTGCACTGCTG
C05_P_Ttr_for_13	AATCGTGCACTGCTGG
C06_P_Ttr_for_14	CGTGCACTGCTGGAAC
C07_P_Ttr_for_15	GCACTGCTGGAACATGC
C08_P_Ttr_for_16	CTGCTGGAACATGCACAG
C09_P_Ttr_for_17	CTGGAACATGCACAGC
C10_P_Ttr_for_18	GAACATGCACAGCGTATTG
C11_P_Ttr_for_19	CATGCACAGCGTATTGC
C12_P_Ttr_for_20	GCACAGCGTATTGCCATTG
C13_P_Ttr_for_21	CAGCGTATTGCCATTGC

Name	Sequence 5'-3'
C14_P_Ttr_for_22	CGTATTGCCATTGCCG
C15_P_Ttr_for_23	ATTGCCATTGCCGGTG
C16_P_Ttr_for_24	GCCATTGCCGGTGAAC
C17_P_Ttr_for_25	ATTGCCGGTGAACTGG
C18_P_Ttr_for_26	GCCGGTGAACTGGGTG
C19_P_Ttr_for_27	GGTGAACTGGGTGCAAG
C20_P_Ttr_for_28	GAACTGGGTGCAAGCC
C21_P_Ttr_for_29	CTGGGTGCAAGCCTGAG
PATCHY forward primers for amplification of TodS	
C28_P_Tod_for_01	ACTGAGAAGAAACAAGCACAGG
C29_P_Tod_for_02	GAGAAGAAACAAGCACAGG
C30_P_Tod_for_03	AAGAAACAAGCACAGGAAAATC
C31_P_Tod_for_04	AAACAAGCACAGGAAAATCTTAACC
C32_P_Tod_for_05	CAAGCACAGGAAAATCTTAACC
C33_P_Tod_for_06	GCACAGGAAAATCTTAACCAG
C34_P_Tod_for_07	CAGGAAAATCTTAACCAGTTGC
C35_P_Tod_for_08	GAAAATCTTAACCAGTTGCAGC
C36_P_Tod_for_09	AATCTTAACCAGTTGCAGCAAC
C37_P_Tod_for_10	CTTAACCAGTTGCAGCAACAAC
C38_P_Tod_for_11	AACCAGTTGCAGCAACAAC
C39_P_Tod_for_12	CAGTTGCAGCAACAACTTG
C40_P_Tod_for_13	TTGCAGCAACAACTTGTG
C41_P_Tod_for_14	CAGCAACAACTTGTGTACG
C42_P_Tod_for_15	CAACAACTTGTGTACGTTTCC
C43_P_Tod_for_16	CAACTTGTGTACGTTTCCC
C44_P_Tod_for_17	CTTGTGTACGTTTCCCGATC
C45_P_Tod_for_18	GTGTACGTTTCCCGATCAG
C46_P_Tod_for_19	TACGTTTCCCGATCAGC
C47_P_Tod_for_20	GTTTCCCGATCAGCTACG
C48_P_Tod_for_21	TCCCGATCAGCTACGATG
C49_P_Tod_for_22	CGATCAGCTACGATGGG
C50_P_Tod_for_23	TCAGCTACGATGGGTGAATTTG
C51_P_Tod_for_24	GCTACGATGGGTGAATTTG
C52_P_Tod_for_25	ACGATGGGTGAATTTGC
C53_P_Tod_for_26	ATGGGTGAATTTGCAGC

Name	**Sequence 5'-3'**
C54_P_Tod_for_27	GGTGAATTTGCAGCCTATATTG
C55_P_Tod_for_28	GAATTTGCAGCCTATATTGC
C56_P_Tod_for_29	TTTGCAGCCTATATTGCACAC
PATCHY reverse primers for amplification of *Ac*PCM	
M029_Ac_rev1	TTCATTAAGAAGACGCTGACG
M030_Ac_rev2	ATTAAGAAGACGCTGACGC
M031_Ac_rev3	AAGAAGACGCTGACGC
M032_Ac_rev4	AAGACGCTGACGCACG
M033_Ac_rev5	ACGCTGACGCACGTCTG
M034_Ac_rev6	CTGACGCACGTCTGCTTTC
M035_Ac_rev7	ACGCACGTCTGCTTTCC
M036_Ac_rev8	CACGTCTGCTTTCCCG
M037_Ac_rev9	GTCTGCTTTCCCGCGC
M038_Ac_rev10	TGCTTTCCCGCGCTCG
M039_Ac_rev11	TTTCCCGCGCTCGTCAG
M040_Ac_rev12	CCCGCGCTCGTCAGCC
M041_Ac_rev13	GCGCTCGTCAGCCAGTAATTC
M042_Ac_rev14	CTCGTCAGCCAGTAATTCATTATG
M043_Ac_rev15	GTCAGCCAGTAATTCATTATGACG
M044_Ac_rev16	AGCCAGTAATTCATTATGACG
M045_Ac_rev17	CAGTAATTCATTATGACGCAGC
M046_Ac_rev18	TAATTCATTATGACGCAGCAC
M047_Ac_rev19	TTCATTATGACGCAGCAC
M048_Ac_rev20	ATTATGACGCAGCACAATTTC
PATCHY reverse primers for amplification of *Av*PCM	
M049_Av_rev1	CTCGTTTAAGACACGCTGAC
M050_Av_rev2	GTTTAAGACACGCTGACGAATG
M051_Av_rev3	TAAGACACGCTGACGAATG
M052_Av_rev4	GACACGCTGACGAATGTC
M053_Av_rev5	ACGCTGACGAATGTCTGC
M054_Av_rev6	CTGACGAATGTCTGCTTTG
M055_Av_rev7	ACGAATGTCTGCTTTGTTACG
M056_Av_rev8	AATGTCTGCTTTGTTACGC
M057_Av_rev9	GTCTGCTTTGTTACGCTCC

Name	Sequence 5'-3'
M058_Av_rev10	TGCTTTGTTACGCTCCTC
M059_Av_rev11	TTTGTTACGCTCCTCTTGC
M060_Av_rev12	GTTACGCTCCTCTTGCATC
M061_Av_rev13	ACGCTCCTCTTGCATCAG
M062_Av_rev14	CTCCTCTTGCATCAGTTCATTATG
M063_Av_rev15	CTCTTGCATCAGTTCATTATGG
M064_Av_rev16	TTGCATCAGTTCATTATGGC
M065_Av_rev17	CATCAGTTCATTATGGCGC
M066_Av_rev18	CAGTTCATTATGGCGCAG
M067_Av_rev19	TTCATTATGGCGCAGAACC
M068_Av_rev20	ATTATGGCGCAGAACC
Primers for cloning of orthogonal TtrSR TCS	
B55_Pttr_BglII_for	CGTTAAAGATCTATATTTGTTGCGCTAGA
B56_Pttr_XbaI_rev	TGCCAGTCTAGAACAGGCATTC
B57_Bb_for_DmTtrSR	ACGTCTGCGTCTGGAAGATAATCGTTAACAATTGATGTAAGTTAGCTCACTCA
B58_Bb_rev_DmTtrSR	CATTCAGCTGACGCTGGGTATTAATCAGCTCACGATTAGCACGCTCTAAG
B59_Ins_for_DmTtrSR	CTTAGAGCGTGCTAATCGTGAGCTGATTAATACCCAGCGTCAGCTGAATG
B60_Ins_rev_DmTtrSR	TGAGTGAGCTAACTTACATCAATTGTTAACGATTATCTTCCAGACGCAGACGT
B84_P_V_sc_for	GGCGTTTCGCCTTTGATATCGCGAACTGATTAATACCCAGCGTCAG
B85_P_V_sc_rev	GCAACTCTGCGTTACGCCCTTCAAGCTCACGATTAGCACGCTCTA
Primers for cloning of orthogonal TodST TCS	
TodX_fw	GCACAAGATCTGGTCTGAGGTTTTCATCGAC
TodX_rv	CGTGCTCTAGAAATTACAATCCTTCCAC
0_pDusk_fw	GAGTCAATTGAGGGTGGTGAATGTGGCTAG
1_TodS_fw	GATATCACCGAGAAGAAACAAGCACAGGAAAATC
2_NoMfeI_rv	CGTACACAAGTTGTTGCTGCAACTGGTTAAGATTTTCCTGTGCTTGTTTC
3_TodS_fw	GCAGCAACAACTTGTGTACGTTTCCCGATC
4_TodT_rv	GCATCAATTGCTATTCCAGGCTATCCTTGAG
5_pDusk_rv	GCTTGTTTCTTCTCGGTGATATCATTCTGAATTC
M014_Av_Bb_rev	GTCAGATCAACGGTCTGGGTTGCAGTCATGCGTGGGCGACCTCAGGC
M015_Av_Ins_for	GCCTGAGGTCGCCCACGCATGACTGCAACCCAGACCGTTGATCTGAC
C26_Bb_for_P_X_sc	ATTCGTCAGCGTGTCTTAAACGAGGTTAACTGAGAAGAAACAAGCACAG
C27_Ins_rev_P_X_sc	CTGTGCTTGTTTCTTCTCAGTTAACCTCGTTTAAGACACGCTGACGAAT

Name	**Sequence 5'-3'**
Primers for cloning StrR variants	
B73_Bb_for_pStrepDusk	GATCACCAAGGTAGTCGGCAAATAAGAATTAATTCATGAGCGGATACATATT
B74_Bb_rev_pStrepDusk	AAGGATCTCAAGAAGATCCTTTGATCTGATGCCTCCGTGTAAGGGG
B75_Ins_for_pStrepDusk	CCCCTTACACGGAGGCATCAGATCAAAGGATCTTCTTGAGATCCTT
B76_Ins_rev_pStrepDusk	AATATGTATCCGCTCATGAATTAATTCTTATTTGCCGACTACCTTGGTGATC
B26_Ins_rev	CGAGATGATAGGAGGTCTAGCATGACGACCAAGGGACATATCTACG
B27_Bb_for	CGTAGATATGTCCCTTGGTCGTCATGCTAGACCTCCTATCATCTCG
M014_Av_Bb_rev	GTCAGATCAACGGTCTGGGTTGCAGTCATGCGTGGGCGACCTCAGGC
M015_Av_Ins_for	GCCTGAGGTCGCCCACGCATGACTGCAACCCAGACCGTTGATCTGAC
Primers for cloning MCS variant	
C76_Bb_for_MCS	ATCAGCAACTACATGAAGGGCTCGCGGCGGCTGCTTGCCG
C77_Ins_rev_MCS	CGGCAAGCAGCCGCCGCGAGCCCTTCATGTAGTTGCTGAT
M014_Av_Bb_rev	GTCAGATCAACGGTCTGGGTTGCAGTCATGCGTGGGCGACCTCAGGC
M015_Av_Ins_for	GCCTGAGGTCGCCCACGCATGACTGCAACCCAGACCGTTGATCTGAC
Primers for cloning lux variants	
lux-op_Nde_for	**GGATCCCATATG** AAATTTGGAAACTTTTTGCTTACATACC
lux-op_Sac_rev	**TGACGAGCTC** TCAACTATCAAACGCTTCG
PfixK2_NdeI_for	**TGACCATATG** ATATCTCCTTCTTAAAGTTAAACAAAATT
PfixK2_rev_OLPmamG	**ACTAAGAGCTAGTAAAGCGAAAAAG** CGGGATCTCGACGCTCTC
DrHo_OLPmamG_for	**CTTTTTCGCTTTACTAGCTCTTAGTTCTCCAATAAATTCCCTGCGAAGCTTAGGAGATCAGTATATG** CTCCGACTCATGATCATGAAGC
FixJ_NotI_rev	**TGACGCGGCCGC** TCAATCGTTGAGCATGCC

Supplementary Table 2

Plasmids used in this study.

ID	Construct	Reference
pBAM2	*p15A* ori, miniTn5, Amp^R, Kan^R	Uebe, unpublished
pBAM2-luxAE	*p15A* ori, miniTn5, Amp^R, Kan^R, *luxABCDE*	(Dziuba et al., 2021)
p*Dm*REDlux	*p15A* ori, miniTn5, Amp^R, Kan^R, PfixK2-*luxABCDE*, PmamDC-*DrhemO-Dmpcm-fixL*	(this study)
p*Av*NIRlux	*p15A* ori, miniTn5, Amp^R, Kan^R, PfixK2-*luxABCDE*, PmamDC-*DrhemO-Avpcm-fixL*	(this study)
pMH005	*Ac*NIRusk-0	(this study)
pMH006	*Av*NIRusk-0	(this study)
pMH008	pCDF-Duet-*Ac*PCM/HO	(this study)
pMH009	pCDF-Duet-*Av*PCM/HO	(this study)
pMH013	*Ac*NIRusk-PATCHY-start construct	(this study)
pMH014	*Av*NIRusk-PATCHY-start construct	(this study)
pMH017	*Ac*NIRusk+16a	(this study)
pMH018	*Ac*NIRusk+16b	(this study)
pMH019	*Ac*NIRusk-1a (*Ac*NIRusk)	(this study)
pMH020	*Av*NIRusk+16b	(this study)
pMH021	*Ac*NIRusk-4	(this study)
pMH023	*Av*NIRusk-1	(this study)
pMH026	pCDF-Duet-*Pa*PCM/HO	(this study)
pMH028	*Av*NIRusk+17a (*Av*NIRusk)	(this study)
pMH029	*Av*NIRusk+16a	(this study)
pMH030	*Av*NIRusk-5	(this study)
pMH034	*Ac*NIRusk-1b	(this study)
pMH038	*Av*NIRusk+17b	(this study)
pMIR66	TodS and TodT proteins	(Ramos-González et al., 2002)
pMIR77	PtodX promoter	(Ramos-González et al., 2002)
pQX037	*Pa*PAC	(Xu et al., 2024)
pQX086	*Av*PAC	(Xu et al., 2024)
pQX091	*Ac*PAC	(Xu et al., 2024)
pRD349	pDusk-YT1-X	(unpublished)

ID	Construct	Reference
pSM001	*Dr*REDusk-MCS	(Multamäki et al., 2022)
pSM003	*Dm*REDusk	(Meier et al., 2024a)
pSM024	*Dm*REDusk-MCS	(Meier et al., 2024a)
pSM087	*Dm*DERusk	(Meier et al., 2024a)
pSM090	*Dm*DERusk-YPet	(Meier et al., 2024a)
pSM091	*Dm*DERusk-MCS	(Meier et al., 2024a)
pSM122	*Dm*DERusk-StrR-YPet	(this study)
pSM123	*Dm*Ttr-REDusk-PATCHY-start construct	(this study)
pSM128	*Av*Tod-NIRusk-PATCHY-start construct	(this study)
pSM136	*Av*NIRusk-StrR-YPet	(this study)
pSM146	*Dm*Ttr-13	(this study)
pSM147	*Dm*Ttr-0	(this study)
pSM148	*Dm*Ttr+5	(this study)
pSM149	*Dm*Ttr+7a	(this study)
pSM150	*Dm*Ttr+7b	(this study)
pSM153	*Dm*Ttr+14	(this study)
pSM160	*Av*Tod+3	(this study)
pSM161	*Av*Tod+16	(this study)
pSM162	*Av*Tod+19	(this study)
pSM163	*Av*Tod+21	(this study)
pSM164	*Av*Tod+26	(this study)
pSM182	*Av*NIRusk-MCS	(this study) Addgene: 235084

Supplementary References

Abramson J, Adler J, Dunger J, Evans R, Green T, Pritzel A, Ronneberger O, Willmore L, Ballard AJ, Bambrick J, Bodenstein SW, Evans DA, Hung C-C, O'Neill M, Reiman D, Tunyasuvunakool K, Wu Z, Žemgulytė A, Arvaniti E, Beattie C, Bertolli O, Bridgland A, Cherepanov A, Congreve M, Cowen-Rivers AI, Cowie A, Figurnov M, Fuchs FB, Gladman H, Jain R, Khan YA, Low CMR, Perlin K, Potapenko A, Savy P, Singh S, Stecula A, Thillaisundaram A, Tong C, Yakneen S, Zhong ED, Zielinski M, Žídek A, Bapst V, Kohli P, Jaderberg M, Hassabis D, Jumper JM. 2024. Accurate structure prediction of biomolecular interactions with AlphaFold 3. *Nature* **630**:493–500. doi:10.1038/s41586-024-07487-w

Dziuba M, Riese CN, Borgert L, Wittchen M, Busche T, Kalinowski J, Uebe R, Schüler D. 2021. The Complex Transcriptional Landscape of Magnetosome Gene Clusters in Magnetospirillum gryphiswaldense. *mSystems* **6**:10.1128/msystems.00893-21. doi:10.1128/msystems.00893-21

Hennemann J, Iwasaki RS, Grund TN, Diensthuber RP, Richter F, Möglich A. 2018. Optogenetic Control by Pulsed Illumination. *Chembiochem* **19**:1296–1304. doi:10.1002/cbic.201800030

Multamäki E, García de Fuentes A, Sieryi O, Bykov A, Gerken U, Ranzani AT, Köhler J, Meglinski I, Möglich A, Takala H. 2022. Optogenetic Control of Bacterial Expression by Red Light. *ACS Synth Biol* **11**:3354–3367. doi:10.1021/acssynbio.2c00259

Meier SSM, Multamäki E, Ranzani AT, Takala H, Möglich A. 2024a. Leveraging the histidine kinase-phosphatase duality to sculpt two-component signaling. *Nat Commun* **15**:4876. doi:10.1038/s41467-024-49251-8

Ramos-González M-I, Olson M, Gatenby AA, Mosqueda G, Manzanera M, Campos MJ, Víchez S, Ramos JL. 2002. Cross-Regulation between a Novel Two-Component Signal Transduction System for Catabolism of Toluene in Pseudomonas mendocina and the TodST System from Pseudomonas putida. *J Bact* **184**:7062–7067. doi:10.1128/jb.184.24.7062-7067.2002

Schmidt A, Sauthof L, Szczepek M, Lopez MF, Escobar FV, Qureshi BM, Michael N, Buhrke D, Stevens T, Kwiatkowski D, von Stetten D, Mroginski MA, Krauß N, Lamparter T, Hildebrandt P, Scheerer P. 2018. Structural snapshot of a bacterial phytochrome in its functional intermediate state. *Nat Commun* **9**:4912. doi:10.1038/s41467-018-07392-7

Stüven B, Stabel R, Ohlendorf R, Beck J, Schubert R, Möglich A. 2019. Characterization and engineering of photoactivated adenylyl cyclases. *Biol Chem* **400**:429–441. doi:10.1515/hsz-2018-0375

Xu Q, Vogt A, Frechen F, Yi C, Küçükerden M, Ngum N, Sitjà-Roqueta L, Greiner A, Parri R, Masana M, Wenger N, Wachten D, Möglich A. 2024. Engineering Bacteriophytochrome-coupled Photoactivated Adenylyl Cyclases for Enhanced Optogenetic cAMP Modulation. *J Mol Biol*, Photosensory Receptors-Mechanisms and Effects **436**:168257. doi:10.1016/j.jmb.2023.168257

Yang X, Kuk J, Moffat K. 2008. Crystal structure of Pseudomonas aeruginosa bacteriophytochrome: Photoconversion and signal transduction. *Proc Natl Acad Sci U S A* **105**:14715–14720.